Lawrence Berkeley National Laboratory
LBL Publications

Title

Instrumentation for the Absorbers in·the Low β* Insertions of the LHC

Permalink

Author

Turner, William C

Publication Date

1998-08-01

LBNL-42180

ERNEST ORLANDO LAWRENCE BERKELEY NATIONAL LABORATORY

Instrumentation for the Absorbers in the Low β* Insertions of the LHC

William C. Turner

Accelerator and Fusion Research Division

DISCLAIMER

Instrumentation for the Absorbers in the Low β* Insertions of the LHC[**]

William C. Turner
Center for Beam Physics
Lawrence Berkeley National Laboratory
University of California
Berkeley, California 94720

August 1998

Instrumentation for the Absorbers in the Low β* Insertions of the LHC**

W.C. Turner
Lawrence Berkeley National Laboratory
Berkeley, CA 94720
13 Aug 1998

ABSTRACT

Concepts are examined for the measurement of luminosity, beam-beam separation and transverse beam shape and size using the high flux of forward neutral particles produced at the low β^* (high luminosity) interaction points (IP's) of the LHC. At design luminosity 10^{34} cm^{-2}sec^{-1} the flux of neutrals striking the neutral beam absorbers (TAN) in front of the D2 beam separation dipoles is high enough (~ 8 neutrons per bunch crossing with mean energy 2.3 TeV) to allow measurement of luminosity with 1% precision in ~ 1.8×10^3 bunch crossings and measurement of beam-beam separation at the collision point with $0.1\sigma^*$ precision in ~ 3×10^4 bunch crossings. An Argon ionization chamber placed near the shower maximum ~ 22 cm inside the Cu neutral beam absorber is analyzed as a possible detector. Background effects due to beam-gas interactions, beam-halo scraping, beam crossing angle modulation and transverse drift of the IP are estimated and found to be small compared to the anticipated signals. Extending these concepts to the front quadrupole absorber (TAS) and segmenting the ionization chambers into four quadrants allows additional measurements of the beam-beam crossing angle and the transverse position of the IP.

1 Introduction

A high flux of forward neutral particles is produced when the 7 TeV proton beams of the LHC are in collision at the high luminosity IP's (IP1 and IP5). Some of these neutrals remain inside the beam pipe until reaching the outer beam separation dipole (D2) located approximately ±150 m from the IP. Absorbers (TAN) are placed just in front of D2 to intercept the energetic neutrals and to prevent their energy deposition from quenching D2 and the outer matching quadrupoles (Q4 to Q6). At design luminosity 10^{34} cm^{-2}sec^{-1} about 210 W is deposited in the neutral absorbers by hadronic and electromagnetic showers as estimated by the MARS13 code.[1,2,3,4] Approximately 90% of these showers are initiated by neutral hadrons (mostly neutrons) and photons and the remaining 10% by charged particles. The neutron energies extend up to the full 7 TeV beam energy and have mean multiplicity m = 0.33 per pp interaction and mean energy 2.3 TeV. For L = 10^{34} cm^{-2}sec^{-1}, 2835 bunches in each ring, 10^{11} p/bunch and total inelastic cross section 80 mb an average of 8.3 neutrons per bunch crossing are incident on the neutral absorber. Since the neutral flux produced by the colliding beams is rather large and proportional to luminosity it is natural to consider placing a detector in the neutral absorbers to infer at least three things: (1) the luminosity, (2) the beam-beam separation at the IP and (3) the transverse beam shape and size. The signal from the detector could be used to feedback regulate variations of the beam-beam closed orbit separation at the IP, due for example to ground motion[5], to a negligible level. The methods that we propose for analysis are similar

to those previously considered for luminosity by van der Meer[6] and for beam-beam centering by Jostlein[7].

A simplified schematic of an interaction region, omitting the lattice components that are not relevant to the discussion, is shown in Fig. 1. In the arcs of LHC the two proton beams circulate in separate beam tubes. Neutral absorbers are placed just inside the outer beam
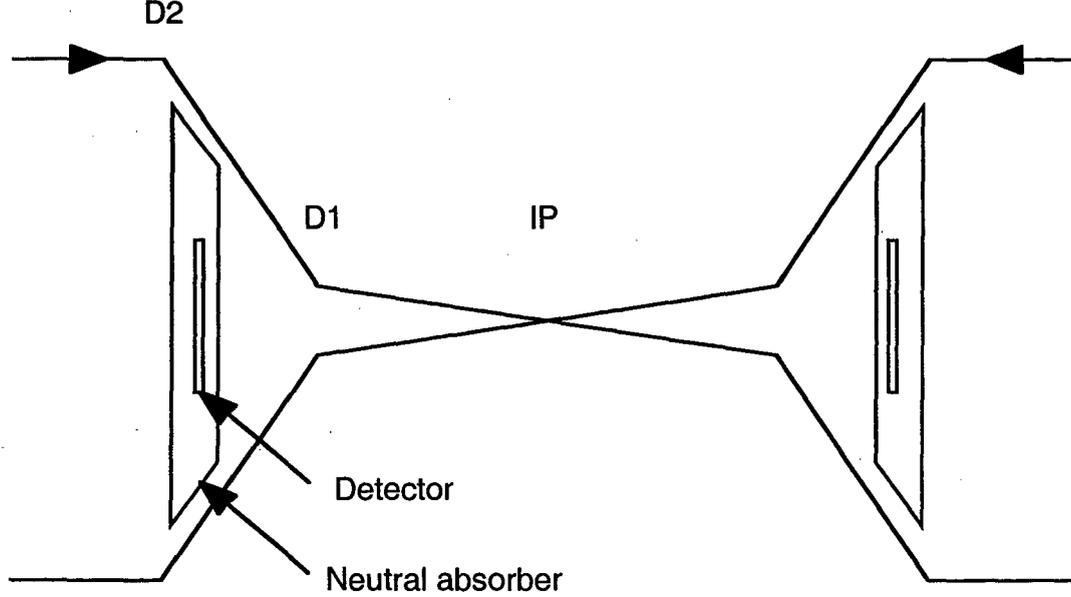
Fig. 1: A schematic of beam crossing in an interaction region.

separation dipoles (D2) and the two beams are inside a single beam tube between absorbers. At the IP the two beams cross at a small angle ~ 300 μrad in order to reduce the effects of parasitic collisions. In the absorbers neutrals are converted into hadronic/electromagnetic showers and the shower energy is mostly deposited by minimum ionizing particles. A suitable detector placed near the shower maximum measures the flux of these ionizing particles which is proportional to the incident neutral flux and therefore the luminosity. At the IP we consider round Gaussian beams with rms beam size in one transverse direction σ_* (= 15.9 μm) with centers separated by a transverse displacement $\vec{D} = D_x \hat{e}_x + D_y \hat{e}_y$. The luminosity is then

$$L = L_0 e^{-\frac{D^2}{4\sigma_*^2}}. \tag{1}$$

Now we suppose that, as indicated in Fig. 2, the transverse displacement is the sum of an intentional time dependent displacement ($\vec{d}(t) = d\cos(\omega t)\hat{e}_x + d\sin(\omega t)\hat{e}_y$) produced by horizontal and vertical (H/V) correctors and a quasi steady-state error

2

$(\vec{\varepsilon} = \varepsilon\,cos(\varphi)\hat{e}_x + \varepsilon\,sin(\varphi)\hat{e}_y).$[7] Assuming the error and intentional displacements are small compared to the rms beam size the luminosity then becomes

$$L = L_0\left(1 - \frac{\varepsilon^2 + d^2}{4\sigma_*^2}\right) - L_0\frac{\varepsilon d}{2\sigma_*^2}cos(\omega t - \varphi). \qquad (2)$$
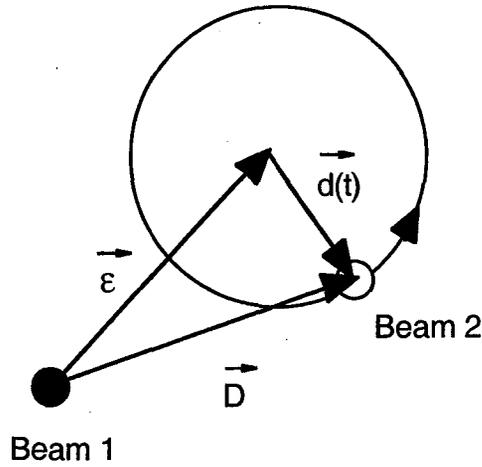
Fig. 2: The beam-beam separation D is the sum of an error ε and an intentional displacement d(t).

The circular sweep $\vec{d}(t)$ has introduced a sinusoidal modulation of luminosity which vanishes when the error offset is reduced to zero. A detector signal proportional to L then has a quasi-static component proportional to L_0 and a time varying component proportional to the scalar product of the error offset $\vec{\varepsilon}$ and the time dependent displacement $\vec{d}(t)$. The time varying component can be used to estimate the magnitude and phase of the error offset and used in a feedback scheme to reduce it to zero. The integration time required to resolve the magnitude of the error offset in the presence of the statistical fluctuations of the quasi-static term will be discussed in the following section.

Once the error offset is reduced to a magnitude that is small compared to the rms beam radius additional information can be obtained. The beam profile and rms beam size in the two transverse dimensions can be measured by changing the sweep to linear polarizations in the x and y planes. If the detector is segmented into four quadrants and combined with a similar detector in the front quadrupole absorber (TAS) the transverse position of the IP and the crossing angle can be measured by using the (left - right)/(left + right) and (up - down)/(up + down) ratios to estimate the centers of the radiation deposition profiles. The absolute measurement of luminosity can be calibrated two ways: (1) against simultaneous measurements of absolute luminosity at the same IP by one of the large detectors (ATLAS or CMS) and (2) by simultaneously measuring the beam size (by the method described) and the beam current and using the usual formula

$$L_0 = \frac{1}{kf}\left(\frac{I}{e}\right)^2 \frac{1}{4\pi\sigma_*^2}$$ (3)

where k is the number of bunches in a beam, f is the revolution frequency and I is the beam current. Eqn. 3 is valid for round Gaussian beams. If the beam profiles found by scanning do not satisfy this assumption then Eqn. 3 can be generalized to treat the actual case.[8] Calibration against the more recently proposed TOTEM experiment for measurement of the elastic and total cross sections can also be considered.[9]

The intentional offset $\vec{d}(t)$ and the feedback offset for compensation of errors are produced by horizontal and vertical dipole correctors (H/V) approximately $\pm\pi/2$ in betatron phase advance from the IP and acting on one of the beams as it approaches and departs the IP. Outgoing H/V correctors are necessary to undo the kick by the ingoing set, thereby avoiding excitation of a betatron oscillation around the machine and interference with the measurement of $\vec{\varepsilon}$.

In the following sections we (1) estimate the statistical errors and the integration times required for the measurements of luminosity and beam-beam separation, (2) summarize the expected magnitudes of power deposition in the neutral absorbers and estimate the fluxes of ionizing particles inside the neutral absorbers, (3) describe the properties of an Argon ionization chamber that is suitable for a detector, (4) analyze the magnitudes of possible background interference with the measurements of luminosity and beam-beam separation and (5) describe the extension of the measurement concepts to the front quadrupole absorber (TAS).

2 Statistical errors of the measurements of luminosity and beam-beam separation

The current from the detector in Fig. 1 may be written as

$$I(t) = e\alpha\varepsilon_{det}m\dot{N}$$
$$= e\alpha\varepsilon_{det}m\sigma_{inel}L$$ (4)

where $\dot{N}$ is the rate of inelastic p-p interactions at the IP, m is the multiplicity of particles falling with the acceptance of the detector per interaction, ε_{det} is the detector efficiency, α the detector gain, and σ_{inel} (= 80 mb) is the inelastic cross section. The gain α defined in Eqn. 4 is the average number of singly charged particles collected per neutral particle initiating a shower within the acceptance of the detector. For an ionization chamber α is the product of the number of minimum ionizing particles crossing the chamber (= α_1) and the number of ion-electron pairs created per minimum ionizing particle (= α_2). These parameters will be calculated below. For the statistical estimates in this report we will include only the neutrons that strike the neutral absorber and ignore the photons.

Integrating Eqn. 4 over a time interval T and assuming Poisson counting statistics for N, α and m and a binomial distribution for ε_{det} readily gives the following expressions for the luminosity and luminosity error. The details of the derivation are given in Appendix A. We assume T is either an integer multiple of or is large compared to $2\pi/\omega$.

$$L_0 = \frac{\int_0^T I(t)dt}{e\alpha\varepsilon_{det}m\sigma_{inel}T} \tag{5}$$

$$\frac{\sigma_L}{L} = \left(\frac{1}{\alpha\varepsilon_{det}m} + \frac{1}{\alpha_1\varepsilon_{det}m} + \frac{1-\varepsilon_{det}}{m\varepsilon_{det}} + \frac{1}{m} + 1\right)^{1/2}\frac{1}{\left(\sigma_{inel}L_0T\right)^{1/2}} \tag{6}$$

Similarly if we multiply Eqn. 4 by $cos(\omega t)$ and $sin(\omega t)$ and integrate we obtain estimates for the components of the displacement error.

$$\varepsilon_x = \varepsilon\cos(\varphi) = \frac{-\int_0^T dt\cos(\omega t)I(t)}{\left(\frac{d}{4\sigma_*^2}\right)e\alpha\varepsilon_{det}m\sigma_{inel}L_0T}$$

$$\varepsilon_y = \varepsilon\sin(\varphi) = \frac{-\int_0^T dt\sin(\omega t)I(t)}{\left(\frac{d}{4\sigma_*^2}\right)e\alpha\varepsilon_{det}m\sigma_{inel}L_0T} \tag{7}$$

The statistical errors of ε_x and ε_y are given by

$$\sigma_{\varepsilon_x}^2 = \frac{1}{2}\left(\frac{4\sigma_*^2}{d}\right)^2\frac{1+\alpha_2+\alpha+\alpha\varepsilon_{det}m}{\alpha\varepsilon_{det}m\sigma_{inel}L_0T}.$$

$$= \sigma_{\varepsilon_y}^2 \tag{8}$$

where again the details of the derivation are in Appendix A. From Eqn. 8 it follows that the errors in the magnitude and phase of $\vec{\varepsilon}$ are given by

$$\sigma_\varepsilon = \left(\sigma_{\varepsilon_x}^2 + \sigma_{\varepsilon_y}^2\right)^{1/2}$$

$$= \left(\frac{4\sigma_*^2}{d}\right)\left(\frac{1 + \alpha_2 + \alpha + \alpha\varepsilon_{det}m}{\alpha\varepsilon_{det}m\sigma_{inel}L_0T}\right)^{1/2} \quad\quad (9)$$

$$\sigma_\varphi = \frac{1}{\sqrt{2}}\frac{\sigma_\varepsilon}{\varepsilon}. \quad\quad (10)$$

From Eqn. 9 we see that the error in the magnitude of the displacement error $\vec{\varepsilon}$ is proportional to the square of the rms beam size in one transverse dimension and inversely proportional to the magnitude of the sweep offset $\vec{d}$. In general we wish to measure $\vec{\varepsilon}$ to some accuracy which insures that the luminosity degradation due to a beam-beam separation error is below some acceptable bound and we would like to perform this measurement in the minimum possible integration time T. According to Eqn. 1 this is equivalent to requiring that the time average of the magnitude of $\vec{D} = \vec{d} + \vec{\varepsilon}$ be bounded by some fraction of the rms beam size. If we choose $\langle D^2 \rangle = 2\delta^2\sigma_*^2$ with $\delta \ll 1$, then

$$\langle D^2 \rangle = \langle d^2 + \varepsilon^2 + 2\vec{d}\cdot\vec{\varepsilon} \rangle$$

$$= d^2 + \sigma_\varepsilon^2 \quad\quad (11)$$

$$= 2\delta^2\sigma_*^2$$

Substituting Eqn. 9 for σ_ε^2 into Eqn. 11 we obtain for the integration time

$$\frac{\alpha\varepsilon_{det}m\sigma_{inel}L_0T}{1 + \alpha_2 + \alpha + \alpha\varepsilon_{det}m} = \frac{4^2}{2\delta^2\dfrac{d^2}{\sigma_*^2} - \dfrac{d^4}{\sigma_*^4}}. \quad\quad (12)$$

Minimizing the integration time given by Eqn. 12 with respect to d gives for the magnitude of sweep offset

$$d = \delta\sigma_*$$

$$= \sigma_\varepsilon \quad\quad (13)$$

and for the integration time,

$$\frac{\alpha\varepsilon_{\text{det}}m\sigma_{inel}L_0T}{1+\alpha_2+\alpha+\alpha\varepsilon_{\text{det}}m} = \frac{4^2}{\delta^4}.$$

(14)

Eqn. 13 says that the optimum choice for the magnitude of the sweep displacement is equal to the allowable rms error of the displacement that has been established from consideration of luminosity degradation. For example if we choose the luminosity degradation due to transverse beam-beam displacement error at the IP to be bounded by $\Delta L/L = 0.5\%$ rms then $\delta = 0.1$, $d = \sigma_\varepsilon = 0.1\sigma_*$ and $\dfrac{\alpha\varepsilon_{\text{det}}m\sigma_{inel}L_0T}{1+\alpha_2+\alpha+\alpha\varepsilon_{\text{det}}m} = 4^2 \times 10^4$.

In Table 1 we estimate the integration time required to achieve statistical errors for measurements of luminosity $\dfrac{\sigma_L}{L} = 0.01$ and of beam-beam displacement $\sigma_\varepsilon = 0.1\sigma_*$. The integration times are given for design luminosity $L_0 = 10^{34}$ cm^{-2}sec^{-1} and expressed in terms of seconds and number of turns (1 turn = 0.089 ms) and bunch crossings which are all consistent with 10^{11} p/bunch, 2835 bunches and 3,564 bunch spaces. The integration times are remarkably short so a neutral absorber based detector clearly has potential usefulness as a storage ring operations tool. For these calculations we have assumed a time dependent displacement amplitude $d = 0.1\sigma_*$ and used Eqns. 6 and 14. The inelastic cross section has been taken to be $\sigma_{inel} = 80$ mb. From Ref. 1 the mean multiplicity of neutral hadrons striking the neutral absorber per pp interaction is $m = 0.33$. For this study we include only the hadrons and leave the refinement of including the photon contribution to the statistical errors for later investigation. The fraction of hadrons that initiate a shower before reaching the detector is $1 - e^{-\frac{l_{\text{det}}}{\lambda_{\text{int}}}} = 1 - e^{-\frac{22}{15.1}} = 0.77$ where we have assumed a detector is placed $l_{det} = 22$ cm inside the absorber and the absorber material is Cu with hadronic interaction length $\lambda_{int} = 15.1$ cm. We assume each of the interacting hadrons is detected so $\varepsilon_{\text{det}} = 0.77$. From Section 3 below we take the detector gain $\alpha = \alpha_1{}^*\alpha_2 = (1.3 \times 10^4){}^*(29.1) = 3.8 \times 10^5$. The values of these parameters that have been used to estimate the integration times are summarized in Table 2.

The discussion so far has implicitly assumed that all bunches are identical; data are accumulated over passages of successive bunches in the bunch train and a single average measurement of luminosity and bunch separation applies to all the bunches in the machine. However the analysis and the integration time in Table 1 when expressed as the number of bunch crossings applies equally well to bunch by bunch measurements provided that a suitable detector and electronics acquisition system can be defined to accumulate the bunch by bunch data. That is, at design luminosity 1,965 turns would be sufficient to measure individually the luminosity of each bunch (and its collision partner) in the machine with 1% precision.

It is easy to extend Table 1 to other cases that can be imagined. To take an extreme case the proposed TOTEM experiment is imagined to operate with 10^{10} p/bunch, 236 bunches and $\beta^* = 1100$ m. Compared to the design luminosity of LHC the luminosity per bunch has been decreased by a factor $(10^{11}/10^{10})^2 \times (1100/0.5) = 2.2 \times 10^5$, so it would take $2.2 \times 10^5 \times 1,965/236 = 1.8 \times 10^6$ turns (2.7 min) to measure average luminosity of all the bunches with 1% precision.

7

Table 1: Estimated integration time for measurement of luminosity and
beam-beam separation with a detector in the neutral absorber.[*]

L	T			T		
	$(\sigma_L/L = .01)$			$(\sigma_\mathcal{E} = 0.1\sigma_*)$		
cm^{-2}sec^{-1}	ms	turns	bunch crossings	ms	turns	bunch crossings
10^{34}	0.062	.69	1,965	.99	11.1	3.1×10^4

[*]For 10^{11} p/bunch, 2835 bunches, 3,564 bunch spaces.

Table 2: Summary of parameters for estimating
the integration times in Table 1.

Parameter	Value
σ_{inel}, (mb)	80
m	0.33
α	3.8×10^5
α_1	1.3×10^4
α_2	29.1
ε_{det}	0.77

3 Argon ionization chamber

3.1 Space charge constraint

According to the results in Table 1 it is necessary to integrate over many bunch
passages in order to obtain reasonable statistical accuracy for measurement of luminosity
and beam-beam separation. Even at the highest luminosity 10^{34} cm^{-2}sec^{-1} it is necessary

to integrate over ~ 0.69 turns (~ 1,965 bunches) to achieve σ_L/L = .01 and 11.2 turns (~ 31,500 bunch passages) to achieve σ_ε = 0.1 $\sigma*$. For measurement of luminosity and beam-beam separation averaged over all the bunches in the machine we can therefore consider a relatively slow detector that integrates over many bunch passages. A parallel plate Argon ionization chamber at atmospheric pressure seems to be a good choice. It is simple and can be constructed for high reliability and high tolerance to radiation damage. Argon has low recombination and is free of electrically induced chemical reactions. We now turn to discussion of the properties of Argon ionization chambers so parameters can be chosen to give a collection current that is linear with the flux of ionizing particles. The main problem to avoid is space charge suppression of the collection current. The saturation curve for an Argon ionization chamber is discussed in detail in Appendix B. The criterion for ensuring that essentially all of the Argon ions and electrons produced by ionization are collected is

$$a \le 2\left(\frac{V}{a}\right)\sqrt{\frac{\varepsilon_0 k^+}{\dot{q}}}$$

(15)

where V is the voltage applied to the plates, a is the plate separation, k_+ is the ion mobility and $\dot{q}$ is the ionization current density in A/cm^3. Gas amplification occurs when the ionization electrons gain enough energy to themselves produce ionization. In Argon at atmospheric pressure this is avoided if V/a < 1.5 kV/cm.

The ionization chamber is assumed to be located approximately 22 cm behind the front face of the absorber so most of the incident hadrons will have interacted, $1 - e^{-22/\lambda int}$ = 0.77, and the detector is near the maximum energy deposited by the hadronic/electromagnetic shower.

3.2 Ionization chamber current

We now proceed to estimate the magnitude of the ionization chamber collection current assuming the electric field strength is low enough that the gas amplification factor is unity. We assume the ionization chamber has square cross section 10 cm x 10 cm and is placed in a gap in the Cu absorber which is near the shower maximum. Fig. 3 is a cross section showing the relative location of the ionization chamber and the beam tubes in the neutral absorber. The center of the incident shower of forward particles is displaced from the symmetry axis of the absorber by a = 2.25 cm due to the crossing angle which has been taken to be ±150 μrad in the horizontal plane. The average power density dP/dm over the face of the ionization chamber is taken to be ~ 5.9 W/kgm at the design luminosity of the LHC.[1] The average flux of minimum ionizing particles F_{mip} incident on the ionization chamber is then

$$F_{mip} = \frac{\left.\dfrac{dP}{dm}\right|_{Cu}}{\left.\dfrac{dE}{dX}\right|_{Cu}}$$

(16)

$$= 2.64 \times 10^{10} \, / \, cm^2 \, / \sec$$

where dP/dm is the power per unit mass deposited in the Cu and $dE/dX = 1.4$ MeV/gm/cm^2 is the specific minimum ionizing energy loss in Cu. Each minimum ionizing particle crossing the Argon chamber produces $N'_{ion/mip}$ ion-electron pairs per cm given by

$$N'_{ion/mip} = \frac{\rho_{Ar} \left.\frac{dE}{dX}\right|_{Ar}}{W_i}$$ (17)

$$= 97 / cm$$

where for Argon we have taken $W_i = 26$ eV, $\left. dE/dX\right|_{Ar} = 1.52 MeV/gm/cm^2$ and $\rho_{Ar} = 1.66 \times 10^{-3} gm/cm^3$ at P = 760 Torr, T = 294 K. The average ionization current density is then

$$\dot{q} = eF_{mip}N'_{ion/mip}$$

$$= 0.41 \, \mu A/cm^3$$ (18)

Allowing a factor of three increase over Eqn. 18 for the maximum ionization density compared to the mean and requiring V/a < 1.0 kV/cm so gas multiplication is negligible, the condition on gap length for avoiding space charge suppression of the collection current given by Eqn. 15 is a < 7.0 mm. Typical parameters for an Argon ionization chamber are given in Table 3. The ion integration time ~ 180μsec = 2 turns given in Table 3 is the electrode gap divided by the ion drift speed. Since the bunch spacing in LHC is 25 nsec, the ions reaching the cathode of the ionization chamber in Table 3 would be integrated over ~ 7,200 bunch spaces. Scaling from the results in Table 2, the rms statistical fluctuations in ion current read out at the cathode would be ~ 0.6%. The electrons move much faster than the ions so their integration time is much shorter ~ 0.6μsec = 6.75x10^{-3} turns. The electron current reaching the anode is integrated over 24 bunch spaces and the corresponding rms statistical fluctuations would be ~8%. The estimated ionization chamber current for both ions and electrons is 12.3 μA for design luminosity 10^{34} cm^{-2}sec^{-1}.
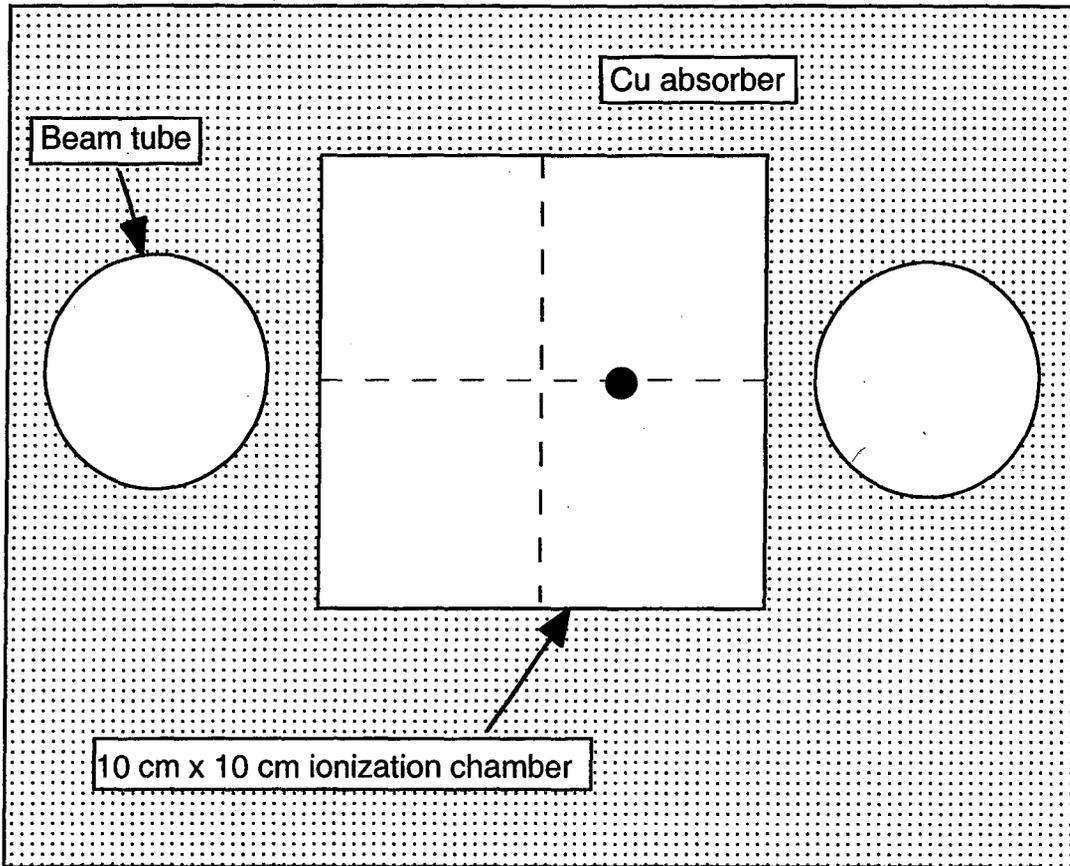
In terms of the parameters defined in this section the ionization chamber collection current can be written as

$$I = eF_{mip}N'_{ion/mip}aA.$$ (19)

The gain α defined in Eqn. 4 is then given by

$$\alpha = \frac{F_{mip}N'_{ion/mip}aA}{\varepsilon_{det}m\sigma_{inel}L}$$ (20)

$$= 3.8 \times 10^5$$

Fig. 3: A cross section 22 cm behind the front face of the neutral absorber located ~ 150 m from the IP showing relative locations of the ionization chamber and beam tubes. The center of the neutral beam induced shower is indicated by the solid black dot and for 150 µrad half crossing angle is about 2.25 cm from the symmetry axis. The Cu absorber extends out to a cross section 25 cm x 30 cm and is surrounded by steel.

where $A = 100$ cm^2 is the area of the collector plates and the other parameters have been defined previously. Eqn. 20 says that on average for each neutral hadron interacting in the Cu in front of the ionization chamber there are 3.8×10^5 Argon ion electron pairs collected. The corresponding number of minimum ionizing particles that produced these Ar$^+$-e$^-$ pairs is $3.8 \times 10^5/(97 \times 0.3) = 1.3 \times 10^4$.

Table 3: Typical parameters for a Neutral Absorber Argon ionization chamber

Parameter	Value
Voltage, kV	0.3
Electrode gap, mm	3
Electrode area, cm^2	100
Current, μA @ $L = 10^{34}\ cm^{-2}sec^{-1}$	12.3
Ion integration time, μs/bunch spaces	180/7,200
Electron integration time, μs/bunch spaces	0.6/24

4 H/V correctors

If H/V correctors are placed at approximately $\pi/2$ phase advance from the IP the kick angle ψ due to the correctors and the transverse displacement x* at the IP are related by

$$x_* = \psi \sqrt{\beta_{H/V} \beta_*}$$ (21)

$\beta_{H/V}$ and β^* (= 0.5 m) are the values of the beta function at the two locations. The product of magnetic field and length of H/V corrector is related to the kick angle by

$$BL = \frac{p}{e}\psi$$ (22)

where p is the proton momentum. If the correctors are located in the ·drift space midway between the Q5 and Q6 matching quadrupoles then $\beta_{H/V}$ = 525 m. Choosing a maximum displacement at the IP x* = σ * = 15.9 μm we obtain BL = 2.3x10^{-2} Tesla-m. This is ten times the kick envisioned for normal operation. A coil radius of 5 cm should allow adequate aperture for the beam even at injection. Choosing a coil length L = 50 cm and assuming the coil is not too strongly coupled to other structure we estimate the stored energy

$$W_B = 2 \times \pi a^2 L \frac{B^2}{2\mu_0}.$$

$$= 6.6 \, J \tag{23}$$

Assuming a cos(θ) coil winding, the number of Ampere turns required is

$$NI_N = 2a \frac{B}{\mu_0} \tag{24}$$

$$= 3.7 \times 10^3 \, A$$

where N is the number of turns and I_N the current. The coil inductance L_N and voltage V are given by

$$\frac{L_N}{N^2} = 964 \, nH \tag{25}$$

$$V_N = L_N \omega I \tag{26}$$

where ω is the driving frequency. If we choose f = 1 kHz and N = 10 turns then L_{10} = 96.4 μH, I_{10} = 370 A and V_{10} = 224 V. Clearly the choices made here are somewhat arbitrary but serve to illustrate that a system exploiting the inherent statistical integration times in Table 1 is practical. We also note that the calculations in this section have been done for a maximum beam displacement equal to σ* at the IP, ten times what would be used in normal operation.

5 Background

In this section we discuss possible backgrounds to the static luminosity measurement and time varying or ac beam-beam separation measurement. At design luminosity $L_0 = 10^{34}$ cm^{-2}sec^{-1} the inelastic pp interaction rate is $\sigma_{inel}L_0 \sim 8 \times 10^8$ sec^{-1}. The amplitude of the ac interaction rate for measurement of beam-beam separation is suppressed by a factor $\epsilon d / 2\sigma_*^2 \sim (0.1)^2 / 2 = 5 \times 10^{-3}$ to 4.0×10^6 sec^{-1}. Potential background rates should be small compared to these rates. So far we have identified five sources of background: (1) beam gas interactions, (2) beam halo interactions with the beam tube in the interaction region, (3) sweeping of the beam crossing angle at the frequency of the beam-beam separation measurement, (4) slow drift of the transverse position of the IP and (5) slow drift of the crossing angle. The first of these background sources is linear in the beam current while the second to fifth are quadratic like the luminosity dependent signals we are trying to measure. The first, fourth and fifth sources of background contribute only to the static luminosity measurement, the second can contribute to both the static and ac measurement while the third contributes only to the ac measurement. Technically what we have listed as the third through fifth sources of background are not really background but are systematic effects that can lead to a misinterpretation of the data.

5.1 Beam gas interactions

An interaction of a 7 TeV proton with a gas molecule in the interaction region can initiate a hadronic/electromagnetic shower that strikes the neutral absorber and contributes a static background signal in the detector. The beam gas interaction rate is given by

$$\dot{N}_{bg} = \frac{I_b}{e} d \sum_j n_j \sigma_{pj} \tag{27}$$

where the summation is over molecular species with density n_j and total cross section σ_{pj} and d is the effective path length for the beam gas interactions to contribute to the background. The relevant gas molecules for the ambient temperature beam tubes in the interaction regions are H_2, CH_4, CO and CO_2. Their partial pressures have been estimated to be 1×10^{-10} Torr, 2×10^{-12} Torr, 1×10^{-11} Torr and 2×10^{-12} Torr respectively.[12,13] For the path length we take the distance between the D1 beam separation dipoles d = 140 m and assume the ~ 30 m lengths of cold vacuum tube through the two sets of Q1-Q3 quadrupoles have the same vacuum as the warm sections which probably overestimates the background. The beam gas interaction rates for design current I_b = 0.54 A are given in Table 4 and sum to 3.5×10^4 sec^{-1}, more than four orders of magnitude less than the beam-beam IP rate 8×10^8 sec^{-1}. Even at 10^{31} cm^{-2}sec^{-1} the ratio of beam gas interaction rate to IP rate is $1.1 \times 10^3 / 8 \times 10^5$ ~ 1/800. The beam gas rate does not become equal to the IP rate until the luminosity falls to 2×10^{25} cm^{-2}sec^{-1}. Beam gas interaction background does not seem to be a concern.

Table 4: Beam gas interaction rate in an IR region.

Molecule	$n_j (cm^{-3})$	$\sigma_{pj} (mb)$	$\dot{N}_{bg,j} (sec^{-1})$
H_2	3.3×10^6	100	1.6×10^4
CH_4	6.6×10^4	600	1.9×10^3
CO	3.3×10^5	810	1.3×10^4
CO_2	6.6×10^4	1220	3.8×10^3
Total			3.5×10^4

5.2 Beam halo interactions with the beam tube

A beam halo is created by small angle elastic scattering of protons at the IP which then diffuse to large radius due to lattice non linearity and beam-beam effects. Most of these halo particles are removed in the beam cleaning insertion. However the beam cleaning system is not completely efficient so some halo particles reach the vacuum tube wall in other parts of the machine. Those that do encounter the beam tube at a small angle of incidence so they may elastically scatter back out of the beam tube surface or their secondary interaction products may escape. These elastically scattered particles and secondaries may then reach the neutral absorber and constitute a background. This background can contribute to both the static luminosity measurement and the ac measurement of beam-beam separation. Fig. 4 indicates schematically how the ac background may arise. In Fig. 4a the circularly swept beam is indicated with a physical aperture limitation on the right. Interaction of the beam halo with the physical object will have a dc term plus an ac term at the fundamental rotation frequency ω. In Fig. 4b a symmetric aperture limitation is placed on the left and the interaction rate is now a sum of a dc component and possibly harmonics of 2ω. However if the beams pass through the aperture off the symmetry axis, as indicated in Fig. 4c, an ac term at the fundamental is restored. Because of the finite crossing angle of the beams this is precisely the situation encountered in the LHC at the locations of the inner triplet quadrupoles and front quadrupole absorber (TAS). In a recent study the limiting aperture in collision optics was found to be the left Q3 quadrupole ~ 47 m from the IP with beam tube radius 30 mm, corresponding to ~ 8σ beam radius allowing for crossing angle and tolerances.[14] The front quadrupole absorbers ~ ±20 m from the IP with beam tube radii 17 mm were only slightly outside this radius at ~8.3 σ. For ±150 μrad crossing angle the two beams are ± 3.0 mm from the symmetry axis of the front quadrupole absorber. However since the phase advance from the IP to the front quadrupole absorbers and inner triplet quadrupoles is very close to $\pi/2$ the amplitude of the centroid modulation of the beam and therefore the ac background signal due to halo scraping should be very small at these locations. We will make a rough estimate below.

At 14 TeV cm the elastic cross section for proton-proton scattering is σ_{elas} ~ 26 mb and protons undergoing elastic scattering feed the beam halo. At design luminosity 10^{34} cm^{-2}sec^{-1} the elastic scattering rate at one IP is 2.6×10^{8} sec^{-1}. With two high luminosity IP's contributing to the halo the rate is 5.2×10^{8} sec^{-1}. Most of these halo particles will be caught by the beam cleaning system; an early study set a requirement for less than 1:400 halo protons to escape the cleaning system and estimated an escape fraction 1:6,500 for a two stage collimation system.[15] The evaluation of this escape fraction is still a subject of study and recent estimates are that it will be in the range 10^{-5} to 10^{-4}.[16] Taking the estimated efficiency 1:6,500 yields a rate $5.2\times10^{8}/6.5\times10^{3} = 8.0\times10^{4}$ sec^{-1} for the beam halo interaction rate with the beam tube in the entire machine excluding the primary collimation system. In a worst case situation all of these protons impact the beam tube of the inner triplet quadrupoles or the front quadrupole absorber and either elastically scatter into or produce energetic secondaries that scatter into the acceptance of the neutral absorber. A background event rate bounded by 8.0×10^{4} sec^{-1} does not seem to pose a problem for the static luminosity measurement or the ac beam-beam separation measurement.

15

(a)

(b)

(c)
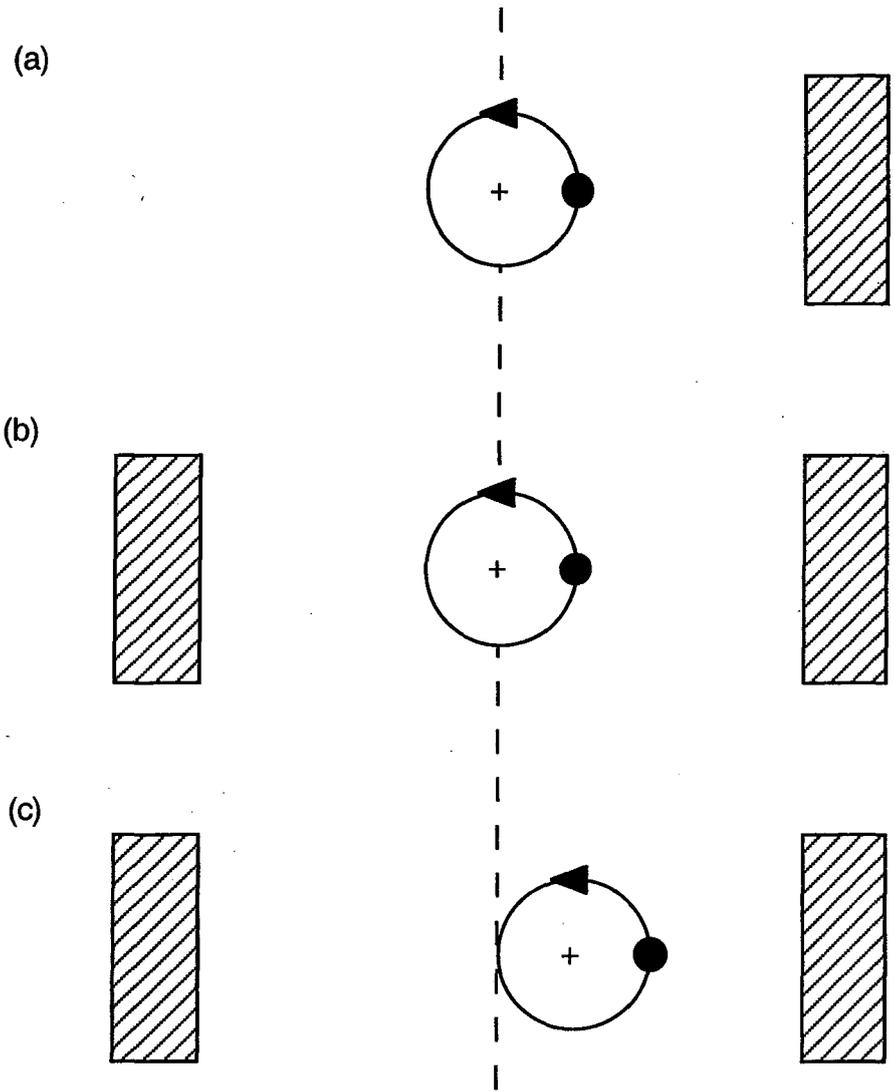
Fig. 4: Illustration of the interaction of the swept beam with physical apertures (a) on one side, (b) symmetrically placed on both sides and (c) asymmetrically placed relative to the center of rotation of the beam.

5.3 Modulation of the beam crossing angle at the frequency of the beam-beam separation measurement

Referring to Fig. 5(a), our assumption has been that the beam-beam separation at the IP varies while the crossing angle is held fixed. In this case the intensity of shower products in the neutral absorber is modulated everywhere in the volume of the absorber by the same

factor as the luminosity changes due to variation of the beam-beam separation at the IP. However if the betatron phase advance of the H/V correctors is not exactly $\pi/2$ from the IP then the crossing angle is modulated as well as the beam-beam separation. This creates an ambiguity in the interpretation of a decreasing signal - is it due to decreasing luminosity or to sweeping the power deposition profile across the detector. Consider an extreme case Fig. 5(b) where the beam-beam separation is zero and only the crossing angle varies. The detector would record an ac signal due to the variation in crossing angle even though the luminosity is constant in this case. A feedback system arranged to minimize the ac modulation of the detector signal would then attempt to steer the beams until the center of the shower intensity coincided with the symmetry axis of the absorber and detector. The increase in static signal would be misinterpreted as an increase in luminosity whereas in reality it only corresponds to optimal placement of the shower on the detector and no change in luminosity. Furthermore the beam crossing would be displaced by 2.25 cm at the IP relative to the center of the beam tube. This is clearly not something we want to do so we next investigate the magnitude of betatron phase error and the ac modulation of the detector signal that it causes.

Ideally the betatron phase advance between the location of the H/V correctors and the IP would be $\pi/2$ and the beam would arrive at the IP with amplitude x* and angle x'* relative to the design orbit given by

$$
\begin{aligned}
x_* &= \psi\sqrt{\beta_{H/V}\beta_*}\sin(\pi/2) \\
&= \psi\sqrt{\beta_{H/V}\beta_*} \\
x'_* &= \psi\sqrt{\frac{\beta_{H/V}}{\beta_*}}\beta'_*\sin(\pi/2) + \psi\sqrt{\frac{\beta_{H/V}}{\beta_*}}\cos(\pi/2) \\
&= 0
\end{aligned}
\tag{28}
$$

where ψ is the magnitude of angular kick given by the H/V corrector and, according to our earlier notation of Eqn. 13, is chosen so that

$$
\psi = 0.1\frac{\sigma_*}{\sqrt{\beta_{H/V}\beta_*}}.
\tag{29}
$$

In the general case where the phase advance between the H/V correctors and the IP is $\pi/2+\Delta\phi$, x* and x'* are given by

17

$$x_* = \psi \sqrt{\beta_{H/V} \beta_*} \sin(\pi/2 + \Delta\phi)$$

$$\approx \psi \sqrt{\beta_{H/V} \beta_*}$$

$$x'_* = \psi \sqrt{\frac{\beta_{H/V}}{\beta_*}} \cos(\pi/2 + \Delta\phi) \qquad (30)$$

$$\approx -\psi \sqrt{\frac{\beta_{H/V}}{\beta_*}} \Delta\phi$$

so the crossing angle as well as the beam position are modulated. The H/V correctors should be located in a non-common part of the machine, where the beams are in separate vacuum tubes, and preferably where the beam tube is warm. However the ideal phase advance of $\pi/2$ occurs in the middle of the D1 beam separation dipole which although warm is in the common part of the machine and not a practical location for the H/V correctors. The two beams are only separated by 2.1 cm in D1. The ~ 30 m drift region between the Q5 and Q6 matching quadrupoles is the closest non-common space to $\pi/2$ phase advance from the IP that is not presently occupied by equipment. At this location the typical phase advance to the IP is $\pi/2 + \Delta\phi$ = 1.684 radians, so $\Delta\phi$ = 0.113 radians = 6.5°. If we evaluate x* and x'* under these conditions we obtain

$$x_* = 0.994\psi \sqrt{\beta_{H/V} \beta_*}$$

$$x'_* = -0.113\psi \sqrt{\frac{\beta_{H/V}}{\beta_*}} \qquad (31)$$

Inserting ψ from Eqn. 29, σ_* = 15.9 μm, β_* = 0.5 m, $\beta_{H/V}$ = 525 m into Eqn. 31 yields

$$x_* = .0994\sigma_*$$

$$= 1.58 \; \mu m$$

$$x'_* = -.0113 \frac{\sigma_*}{\beta_*} \qquad (32)$$

$$= 0.36 \; \mu rad$$

The modulation of the crossing angle by x'* causes the center of the neutral deposition profile to move transversely by 0.36x150 = 54 μm at the front face of the neutral absorber.

18
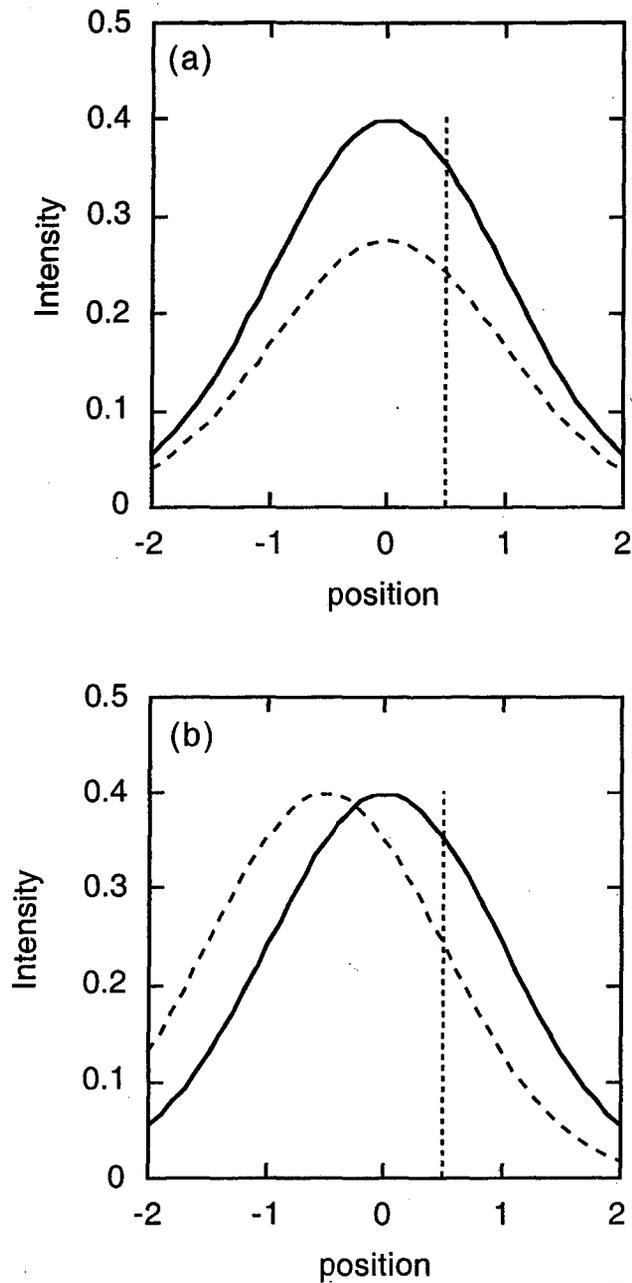
Fig.5: Variation of signal with (a) variation of beam-beam separation with crossing angle fixed and (b) variation of crossing angle with beam-beam separation fixed. A detector located at the vertical dotted line would not distinguish between these two cases. The units of the horizontal and vertical axes are purely arbitrary and for qualitative illustration only.

In order to estimate the importance of the size of the crossing angle variation given by Eqn. 32 it is necessary estimate how the changing power deposition profile in the neutral absorber affects the luminosity signal. The flux of minimum ionizing particles near the axial shower maximum and for r < 10 cm may be approximated by a Gaussian function

$$G = G_0 e^{-\frac{r^2}{2\sigma^2}}$$

(33)

where $G_0 = 6.25 \times 10^{10}$ mip/cm^2, $\sigma = 3.0$ cm and r is measured from the center of the power deposition profile. For the nominal half crossing angle 150 μrad and a distance L ~ 150 m from the IP, the center of the shower symmetry axis is 2.25 cm from the symmetry axis of the detector in Fig. 3. The detector signal is proportional to the integral of the flux of minimum ionizing particles over the surface of the detector. Assuming a displacement of the shower axis by a distance a in the transverse x direction we obtain for the flux S(a) and its derivative

$$S(a) = G_0 \int_{-y_m}^{y_m} e^{-\frac{y^2}{2\sigma^2}} dy \int_{-x_m}^{x_m} e^{-\frac{(x-a)^2}{2\sigma^2}} dx$$

$$= 2\pi\sigma^2 G_0 \left(2F\left(\frac{y_m}{\sigma}\right) - 1 \right) \times \left(F\left(\frac{x_m - a}{\sigma}\right) + F\left(\frac{x_m + a}{\sigma}\right) - 1 \right)$$

(34)

$$\frac{dS}{da} = -\sqrt{2\pi}\sigma G_0 \left(2F\left(\frac{y_m}{\sigma}\right) - 1 \right) \times \left(e^{-\frac{(x_m - a)^2}{2\sigma^2}} - e^{-\frac{(x_m + a)^2}{2\sigma^2}} \right)$$

where

$$F(x_m) = \int_{-\infty}^{x_m} e^{-\frac{x^2}{2}} \frac{dx}{\sqrt{2\pi}}$$

(35)

is the tabulated Gaussian probability integral. We then estimate the amplitude of signal modulation due to the crossing angle variation given by Eqn. 32,

$$\frac{\delta I}{I} = \frac{1}{S(a)}\frac{dS}{da}Lx'_*$$

$$= \frac{1}{\sqrt{2\pi}\sigma}\left(\frac{e^{-\frac{(x_m-a)^2}{2\sigma^2}} - e^{-\frac{(x_m+a)^2}{2\sigma^2}}}{F\left(\frac{x_m-a}{\sigma}\right) + F\left(\frac{x_m+a}{\sigma}\right) - 1}\right)Lx'_* \qquad (36)$$

$$= 5.3x10^{-4}$$

where we have taken a = 2.25 cm, s = 3.0 cm, L = 150 m and x'$_m$ = 0.36 μrad. The result given by Eqn. 36 is one order of magnitude less than the modulation we have discussed for nulling the beam-beam offset to 0.1σ* given by

$$\frac{\delta I}{I} = \frac{\varepsilon d}{2\sigma_*^2}$$

$$= \frac{(0.1)^2}{2} \qquad (37)$$

$$= 5\times10^{-3}$$

5.4 Slow drift of the beam crossing angle and transverse position of the IP

The last two background effects mentioned at the beginning of this section are slow drifts of the crossing angle and transverse position of the IP on a time scale t >> 1/ω. A drift this slow would not interfere with measurement of transverse separation of the two beams at the IP but would lead to spurious increases or decreases in the "static" luminosity measurement due to the profile effect sketched in Fig. 5. It is a simple matter to estimate the size of these effects using Eqn. 36 and normalizing drifts in crossing angle (δψ) to μrad and in transverse position (δx)to μm. We then obtain

$$\frac{\delta I}{I} = 1.5x10^{-3}\delta\psi(\mu rad) \qquad (38)$$

for change in crossing angle with no change in transverse position of the IP and

$$\frac{\delta I}{I} = 1.0x10^{-5}\delta a(\mu m) \qquad (39)$$

for change in transverse position with the crossing angle held fixed. Long term drifts of the order ~ 1 μrad in crossing angle and ~ 1 μm in transverse position of the IP will therefore cause no difficulty with measurement of luminosity to the level of ~ 1% precision. The

detector is more sensitive to variation of crossing angle than to variation of transverse position of the IP owing to the distance (~ 150 m) of the detector from the IP.

We conclude from this discussion that background effects that have so far been examined are not serious concerns for the proposed measurement of luminosity and control of beam-beam displacement. The signal and background rates are summarized in Table 5.

Table 5: Summary of signal and estimated background rates at design
luminosity 10^{34} cm^{-2}sec^{-1}

Signal	Rate (sec-1)	Background effects	Rate (sec-1)
Inelastic collisions at IP	8×10^8	Beam gas collisions	3.5×10^4
		Beam halo collisions	8×10^4
		1µm slow drift of IP	8×10^3
		1µrad slow drift of half crossing angle	1.2×10^6
ac modulation amplitude for 0.1σ* beam sweep	4×10^6	ac crossing angle modulation	4×10^5
		ac beam halo collisions	$< 8 \times 10^4$

6 Extensions

The concepts that have been discussed so far can be extended in several directions: (1) instrumenting the front quadrupole absorber (TAS), (2) segmenting the detector to allow measurement of the beam-beam crossing angle and transverse position of the IP and (3) improving the time resolution so that bunch by bunch measurements are possible. We leave the third of these to later investigation and discuss the first two below.

6.1 Front quadrupole absorber

The function of the front quadrupole absorber is similar to the neutral absorber - to protect superconducting magnets from the intense flux of collision products from the IP. The front quadrupole absorber fits tightly around the beam tube and is located ~ 20 m from the IP, just in front of the first inner triplet quadrupole Q1. The absorber is a 50 cm OD, 1.8 m long piece of Cu. At 10^{34} cm^{-2}sec^{-1} luminosity ~ 270W is deposited in the front quadrupole absorber, again calculated with the MARS13 code.[1,2,3,4] Approximately 90% of the power is due to charged pions and photons and the remaining 10% due to neutral hadrons and protons. At design luminosity 10^{34} cm^{2}sec^{-1} the mean multiplicity of charged pions is 6.8 per bunch crossing with mean energy 159 GeV; the corresponding numbers for photons are 8.3 per bunch crossing and 87 GeV. We follow the same approach as for the neutral absorber, locating an ionization chamber near the shower maximum ~ 20 cm behind the front face of the front quadrupole absorber. For statistical calculations we assume the fluctuations are dominated by the hadrons - in this case the charged pions. Since the mean multiplicity of the pions incident on the front quadrupole absorber is ~ 20 times higher than the means number of neutrons incident on the neutral absorber we may expect the integration times are reduced by a factor of ~ 4.5 for a specified precision. In
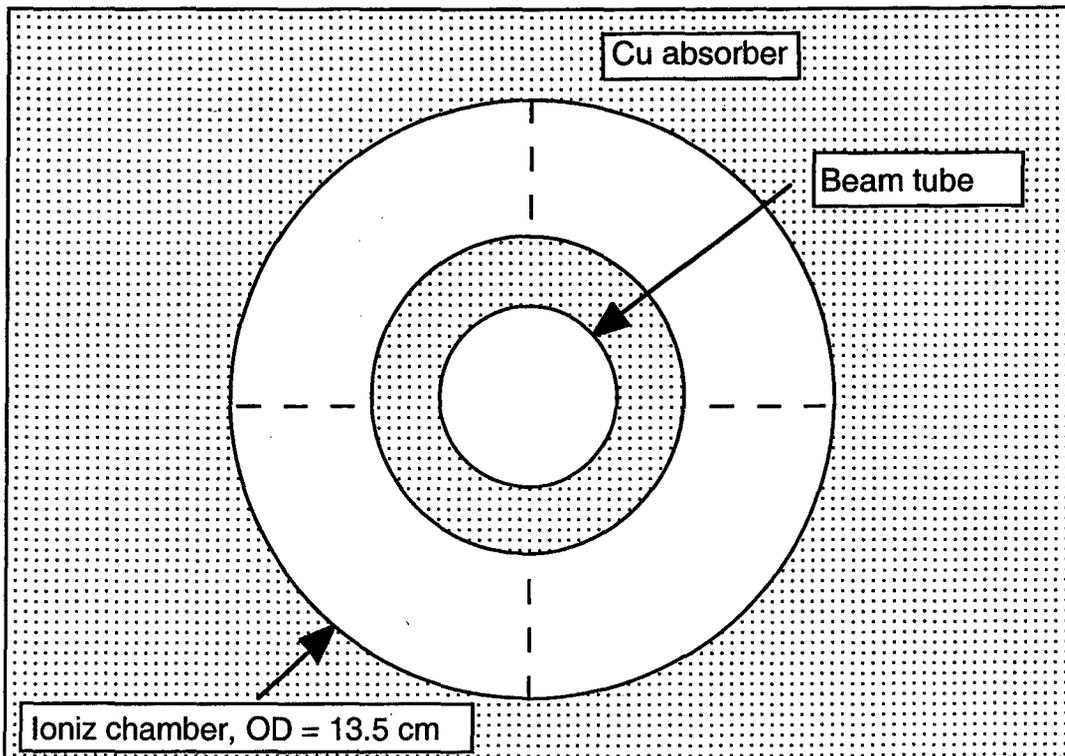
Fig. 6: A cross section 20 cm behind the front face of the front quadrupole absorber located ~ 20 m form the IP showing relative locations of the beam tube and ionization chamber. The Cu absorber extends out to a radius ~ 25 cm.

addition a front quadrupole absorber detector would be ~ 150/20 times less sensitive to the crossing angle effects discussed in Section 5 for the neutral absorber. The disadvantage of the front quadrupole location is that it is surrounded by massive shielding for the ATLAS and CMS detectors and therefore more inaccessible than a detector in the neutral absorber. A sketch of an ionization chamber imbedded ~ 20 cm inside the Cu of the front quadrupole absorber is shown in Fig. 6. It has circular cross section with inside radius 3.5 cm, outside radius 6.75 cm and area ~ 105 cm^2.

The calculation of integration time for 1% luminosity measurement and 0.1s* measurement of beam-beam separation given in Section 2 for the neutral absorber ionization chamber has been repeated for the front quadrupole absorber. The results are given in Table 6 and parameters summarized in Table 7. The average power density over the face of the ionization chamber has been taken to be 1.83 W/kgm, the electrode gap is 3 mm and the ionization chamber current at luminosity 10^{34} $cm^{-2}sec^{-1}$ is 4.0 μa.

Table 6: Estimated integration time for measurement of luminosity and beam-beam separation with a detector in the front quadrupole absorber.[*]

L	T ($\sigma_L/L = .01$)			T ($\sigma_\varepsilon = 0.1\sigma_*$)		
cm^{-2}sec^{-1}	ms	turns	bunch crossings	ms	turns	bunch crossings
10^{34}	0.015	0.17	482	0.24	2.7	7,655

[*]For 10^{11} p/bunch, 2835 bunches, 3,564 bunch spaces.

Table 7: Summary of parameters for estimating the integration times in Table 6.

Parameter	Value
σ_{inel}, (mb)	80
m	6.8
α	6.25×10^3
α_1	215
α_2	29.1
ε_{det}	0.73

6.2 Segmentation

As noted in Section 5 the signals in the absorber detectors are sensitive to the crossing angle and transverse position of the interaction point. This can be turned to advantage by segmenting the detectors into quadrants and using the (left - right)/(left+right) and (up-down)/(up+down) ratios to calculate the center of the power deposition profiles. If the neutral absorber and front quadrupole absorber are both instrumented this way then this information can be used to estimate the crossing angle and the transverse location of the interaction point. In this section we estimate the sensitivity of the detectors for these type of measurements.

6.2.1 Neutral absorber

To good approximation the flux of minimum ionizing particles crossing the ionization chamber in the TAN may be represented by

$$F^N_{mip} = F^N_{mip,0} e^{-\frac{(x-a_n)^2}{2\sigma^2} - \frac{y^2}{2\sigma^2}} \tag{40}$$

where $\sigma = 3.0$ cm, the center of the profile has been assumed to be displaced by a distance a_n in the horizontal plane due to finite crossing angle and the peak flux is $F^N_{mip,0} = 6.25 \times 10^{10}$ cm^{-2}sec^{-1}. Integrating over the area of the ionization chamber we then obtain for the asymmetry ratio

$$R_N = \frac{\int_0^{x_m} e^{-\frac{(x-a_n)^2}{2\sigma^2}} - \int_{-x_m}^0 e^{-\frac{(x-a_n)^2}{2\sigma^2}}}{\int_0^{x_m} e^{-\frac{(x-a_n)^2}{2\sigma^2}} + \int_{-x_m}^0 e^{-\frac{(x-a_n)^2}{2\sigma^2}}}$$

$$= \frac{F\left(\frac{x_m-a_n}{\sigma}\right) + 2F\left(\frac{a_n}{\sigma}\right) - F\left(\frac{x_m+a_n}{\sigma}\right)}{F\left(\frac{x_m-a_n}{\sigma}\right) + F\left(\frac{x_m+a_n}{\sigma}\right) - 1} \tag{41}$$

$$= 0.453$$

where we have taken $x_m = \pm 5$ cm, $a_n = 2.25$ cm (crossing angle = 150 μrad) for the numerical evaluation. The functions in the second row of Eqn. 41 are Gaussian probability integrals defined by Eqn. 35. Similarly we obtain for the derivative of R with respect to the center of the profile,

$$\sqrt{2\pi}\sigma\frac{dR_N}{da_n} = \frac{2 - e^{-\frac{(x-a_n)^2}{2\sigma^2}} - e^{-\frac{(x+a_n)^2}{2\sigma^2}}}{F\left(\frac{x_m - a_n}{\sigma}\right) + F\left(\frac{x_m + a_n}{\sigma}\right)}$$

$$+ \frac{F\left(\frac{x_m - a_n}{\sigma}\right) - F\left(\frac{x_m + a_n}{\sigma}\right) + 2F\left(\frac{a_n}{\sigma}\right) - 1}{F\left(\frac{x_m - a_n}{\sigma}\right) + F\left(\frac{x_m + a_n}{\sigma}\right) - 1} \times \left(e^{-\frac{(x-a_n)^2}{2\sigma^2}} - e^{-\frac{(x+a_n)^2}{2\sigma^2}} \right)$$

$$\frac{dR_N}{da_n} = 0.252 \ cm^{-1}$$

(42)

The rms errors of R_N and the center of the power deposition profile a_n are then related to the rms error of luminosity by

$$\sigma_{R_N} = \frac{1}{\sqrt{2}}\left(1 - R_N^2\right)\frac{\sigma_L}{L}$$

$$= 0.56\frac{\sigma_L}{L}$$

$$\sigma_{a_n} = \frac{1}{\frac{dR_N}{da}}\sigma_{R_N} \qquad .$$

$$= 2.22\frac{\sigma_L}{L} \ cm$$

(43)

6.2.2 Front quadrupole absorber

The calculation of Eqns. 40 - 43 may be repeated for the location of the center of the power deposition profile in the front quadrupole absorber. However an analytic formula approximating the flux of minimum ionizing particles crossing the front quadrupole ionization chamber is different than Eqn. 40 and is given by

$$F_{mip}^S = F_{mip,0}^S e^{-\beta\sqrt{r - a_s}}$$

(44)

with $F_{mip,0}^S = 8.7 \times 10^{11} \ cm^{-2}sec^{-1}$, $\beta = 2.0 \ cm^{-1/2}$, a_s the center of the profile. Assuming $a_s \ll a_1, a_2$ where $a_1 (= 3.5 \ cm)$ and $a_2 (= 6.75 \ cm)$ are the inner and outer radii of the ionization chamber, Eqns. 41 and 42 are replaced by

$$R_S = 0.34 a_s$$
$$= 0.10 \tag{45}$$
$$\frac{dR_S}{a_s} = 0.34 \ cm^{-1}$$

where we have taken $a_s = 0.3$ cm (crossing half angle $= 150$ μrad) for numerical evaluation. We then have for the statistical errors of R_S and a_s,

$$\sigma_{R_S} = 0.7 \frac{\sigma_L}{L}$$
$$\tag{46}$$
$$\sigma_{a_s} = 2.06 \frac{\sigma_L}{L} \ cm$$

6.2.3 Crossing angle and transverse position of the IP

The center of the forward power deposition profile may be represented in the plane of the crossing angle by $a(s) = a_0 + s\psi$ where a_0 is the transverse position of the IP at the crossing point, ψ is the crossing angle and s is the distance from the IP. Measuring a(s) at the two positions corresponding to the front quadrupole absorber and the neutral absorber then gives the following estimates of a_0, y and their errors.

$$a_0 = \frac{L_N}{L_N - L_S} a_s - \frac{L_S}{L_N - L_S} a_n$$

$$\sigma_a = \left(\left(\frac{L_N}{L_N - L_S} \right)^2 \sigma_{a_s}^2 + \left(\frac{L_S}{L_N - L_S} \right)^2 \sigma_{a_n}^2 \right)^{1/2}$$

$$\tag{47}$$

$$\psi = \frac{a_n - a_s}{L_N - L_S}$$

$$\sigma_\psi = \frac{1}{L_N - L_S} \left(\sigma_{a_s}^2 + \sigma_{a_n}^2 \right)^{1/2}$$

Inserting $L_S = 20$ m, $L_N = 150$ m and the results given by Eqns. 43 and 46 into Eqn. 47 we obtain

$$\sigma_{a_0}(mm) = \left(\left(564 \left(\frac{\sigma_L}{L} \right)_S^2 \right) + 11.7 \left(\frac{\sigma_L}{L} \right)_N^2 \right)^{1/2}$$

$$\cong 23.7 \left(\frac{\sigma_L}{L} \right)_S \qquad\qquad (48)$$

$$\sigma_\psi(\mu rad) = 158 \left(\left(\frac{\sigma_L}{L} \right)_S^2 + 1.16 \left(\frac{\sigma_L}{L} \right)_N^2 \right)^{1/2}$$

7 Acknowledgment

8 References

[1] N. Mokhov and G. Stevenson, "Radiation Considerations in the Design of the Neutral Dump Close to the LHC Interaction Regions", CERN/TIS-RP/IR/94-17(1994). This reference is an early calculation. The radiation deposition numbers used in this report have been obtained more recently by N. Mokhov for the v5.0 lattice and reported in ref. 3. The details of the LHC machine design will continue to evolve but are not important for the conclusions of this paper.

[2] The Yellow Book - "The Large Hadron Collider Conceptual Design", CERN/AC/95-05, pg. 49. A power 330 W of neutrals in each direction is quoted in this reference. The discrepancy with the power assumed in this report is not important for the conclusions that are reached.

[3] E. Hoyer, W. Turner and N. Mokhov, "Absorbers for the High Luminosity Insertions of the LHC", LBNL-41964, Proc. of EPAC98, Stockholm (1998).

[4] N.V. Mokhov, "The MARS Code System Users Guide", Fermilab-FN-628(1995).

[5] L.Vos, "Effect of Very Low Frequency Ground Motion on the LHC", Proc. of EPAC98, Stockholm (1998).

[6] S. van der Meer, "Calibration of the Effective Beam Height in the ISR", CERN, ISR, PO/68-31 (1968).

[7] H. Jostlein, "Automatic Beam Centering at the SSC Interaction Regions", Fermilab, TM-1253 (1984).

[8] K. Potter, "Luminosity Measurements and Calculations", Proc. of CERN Accelerator School, S. Turner, ed., CERN 94-01, vol. 1, 117(1994).

[9] W. Kienzle et al, "TOTEM, Total Cross Section, Elastic Scattering and Diffraction Dissociation at the LHC", CERN/LHCC 97-49 (15 Aug 1997).

[10] P.R. Bevington, "Data Reduction and Error Analysis for the Physical Sciences", McGraw-Hill Book Company, New York (1969).

[11] J. W. Boag and T. Wilson, Brit. J. of App. Phys., 3, 222 (1952).

[12] A. Mathewson, C. Reymermier and S. Zhang, "The ATLAS Vacuum System", CERN Vac. Tech. Note 95-22 (Nov 1995).

[13] I. Collins, A. Mathewson and S. Zhang, "The Vacuum System of the Low-Beta Absorbers in ATLAS", CERN Vac. Tech. Note 96-06 (Apr. 1996).

[14] J.B. Jeanneret and R. Ostojic, "Geometrical Acceptance in LHC Version 5.0", LHC Project Note 111 (15 Sep 1997).

[15] The Pink Book - "Design Study of the Large Hadron Collider (LHC)", The LHC Study Group, CERN 91-03 (May 1991).

[16] J.B. Jeanerret, private communication.

9 Appendix A: Derivation of the statistical errors of the measurements of luminosity and beam-beam displacement

In this Appendix we derive the formulas for the statistical errors that are used in Section 2. The starting point is Eqn. 4

$$I(t) = e\alpha\varepsilon_{det}m\dot{N}$$
$$= e\alpha\varepsilon_{det}m\sigma_{inel}L \tag{4}$$

which is integrated over a time interval T to obtain

$$\int_0^T I(t)dt = e\alpha\varepsilon_{det}mN. \tag{A1}$$

For application to an ionization chamber the gain parameter α is the product of the number of minimum ionizing particles passing through the chamber ($= \alpha_1$) and the number of ion-electron pairs produced by each minimum ionizing particle ($= \alpha_2$). Since fluctuations in α_1, α_2, efficiency ε_{det}, multiplicity m and number of pp interactions N are uncorrelated the rms fluctuation in the integrated current is related to the rms fluctuations of these quantities by

$$\sigma_{\int Idt}^2 = (e\alpha_2\varepsilon_{det}mN)^2\sigma_{\alpha_1}^2 + (e\alpha_1\varepsilon_{det}mN)^2\sigma_{\alpha_2}^2 + (e\alpha_1\alpha_2mN)^2\sigma_{\varepsilon_{det}}^2$$
$$+ (e\alpha_1\alpha_2\varepsilon_{det}N)^2\sigma_m^2 + (e\alpha_1\alpha_2\varepsilon_{det}m)^2\sigma_N^2 \tag{A2}$$

We assume α_1, α_2, m and N have Poisson distributions and ε_{det} has a binomial distribution. The various rms quantities are then given by[10]

$$\sigma_{\alpha_1}^2 = \frac{\alpha_1}{\varepsilon_{det}mN} \tag{A3}$$

$$\sigma_{\alpha_2}^2 = \frac{\alpha_2}{\alpha_1\varepsilon_{det}mN} \tag{A4}$$

$$\sigma_{\varepsilon_{det}}^2 = \frac{\varepsilon_{det}(1-\varepsilon_{det})}{mN} \tag{A5}$$

$$\sigma_m^2 = \frac{m}{N} \qquad\qquad (A6)$$

$$\sigma_N^2 = N. \qquad\qquad (A7)$$

We note that for a given integration over N pp interactions, α_2 is sampled $\alpha_1 \varepsilon_{det} mN$ times, $\alpha_1 \varepsilon_{det} mN$ times, $\varepsilon_{det} mN$ times, m N times and N once thus reducing the rms errors by these factors compared to the parent distributions. Since luminosity L is proportional to $\int Idt$ we then obtain for the error of luminosity measurement

$$\frac{\sigma_L^2}{L^2} = \frac{\sigma_{\int Idt}^2}{\left(\int Idt\right)^2}$$

$$= \frac{1}{\alpha_1\alpha_2\varepsilon_{det}mN} + \frac{1}{\alpha_1\varepsilon_{det}mN} + \frac{\left(1-\varepsilon_{det}\right)}{\varepsilon_{det}mN} + \frac{1}{mN} + \frac{1}{N}. \qquad (A8)$$

$$= \frac{1}{\alpha_1\alpha_2\varepsilon_{det}mN} + \frac{1}{\alpha_1\varepsilon_{det}mN} + \frac{1}{\varepsilon_{det}mN} + \frac{1}{N}$$

which with $N = \sigma_{inel}L_0 T$ leads to Eqn. 6 in Section 2. To obtain the error for measurement of the component of beam-beam displacement ε_x we multiply Eqn. 4 by $\cos(\omega t)$, integrate and replace the integral by a discrete sum

$$\varepsilon_x = \frac{-\int_0^T dt\cos(\omega t)I(t)}{\left(\dfrac{d}{4\sigma_*^2}\right)e\alpha_1\alpha_2\varepsilon_{det}m\sigma_{inel}L_0T}$$

$$= \frac{-\sum_j \cos(\omega t_j)I(t_j)\Delta t}{\left(\dfrac{d}{4\sigma_*^2}\right)e\alpha_1\alpha_2\varepsilon_{det}m\sigma_{inel}L_0T} \qquad (A9)$$

The rms fluctuation of ε_x is then related to the fluctuations of current in each bin by

$$\sigma_{\varepsilon_x}^2 = \frac{\sum_j \cos^2(\omega t_j)\sigma_{I_j\Delta t}^2}{\left[\left(\frac{d}{4\sigma_*^2}\right)e\alpha_1\alpha_2\varepsilon_{det}m\sigma_{inel}L_0T\right]^2} \qquad (A10)$$

where

$$I(t_j)\Delta t = e\alpha_1\alpha_2\varepsilon_{det}mN_j \qquad (A11)$$

with N_j equal to the number of pp interactions occurring from t_j to $t_j + dt$. Following the same type of argument leading to Eqn. A8 then gives the following expressions for the rms fluctuation in $\int Idt$ and ε_x

$$\sigma_{I_j\Delta t}^2 = e^2\alpha_1\alpha_2\varepsilon_{det}mN_j(1 + \alpha_2 + \alpha_1\alpha_2 + \alpha_1\alpha_2\varepsilon_{det}m) \qquad (A12)$$

$$\begin{aligned}
\sigma_{\varepsilon_x}^2 &= \left(\frac{4\sigma_*^2}{d}\right)^2 \frac{\alpha_1\alpha_2\varepsilon_{det}m(1 + \alpha_2 + \alpha_1\alpha_2 + \alpha_1\alpha_2\varepsilon_{det}m)}{(\alpha_1\alpha_2\varepsilon_{det}m\sigma_{inel}L_0T)^2}\sum_j \cos^2(\omega t_j)N_j \\
&\approx \left(\frac{4\sigma_*^2}{d}\right)^2 \frac{\alpha_1\alpha_2\varepsilon_{det}m(1 + \alpha_2 + \alpha_1\alpha_2 + \alpha_1\alpha_2\varepsilon_{det}m)}{(\alpha_1\alpha_2\varepsilon_{det}m\sigma_{inel}L_0T)^2}\sum_j \frac{1}{2}N\frac{\Delta t}{T} \qquad (A13) \\
&= \frac{1}{2}\left(\frac{4\sigma_*^2}{d}\right)^2 \frac{\alpha_1\alpha_2\varepsilon_{det}m(1 + \alpha_2 + \alpha_1\alpha_2 + \alpha_1\alpha_2\varepsilon_{det}m)}{(\alpha_1\alpha_2\varepsilon_{det}m\sigma_{inel}L_0T)^2}N
\end{aligned}$$

With $N = \sigma_{inel}L_0T$ and by symmetry $\sigma_{\varepsilon_x} = \sigma_{\varepsilon_y}$ we obtain Eqn. 8.

$$\sigma_{\varepsilon_x}^2 = \sigma_{\varepsilon_y}^2 = \frac{1}{2}\left(\frac{4\sigma_*^2}{d}\right)\frac{(1 + \alpha_2 + \alpha_1\alpha_2 + \alpha_1\alpha_2\varepsilon_{det}m)}{\alpha_1\alpha_2\varepsilon_{det}m\sigma_{inel}L_0T} \qquad (A14)$$

10 Appendix B: Derivation of the saturation curve and collection efficiency of an Argon ionization chamber

For the luminosity measurements discussed in this paper it is essential that the Argon ionization chamber current be a linear function of the incident flux of ionizing radiation. The ionization chamber must therefore operate in the saturation regime where nearly all of the Argon ions and electrons reach the collection plates before recombining. This condition,

32

given by Eqn. 25 above, was derived by Boag and Wilson long ago[7] and is in good agreement with experimental data. Because the saturation condition is usually not discussed in the modern references on particle detection and it is important for our application we outline the derivation in this Appendix.

Let a voltage V_0 be applied to the plates of a parallel plate ionization chamber with plate separation a and filled with an atmospheric pressure of Argon. If E is the electric field between the plates and ρ_+, ρ_- are the densities of Argon ions and electrons respectively then Poisson's equation is

$$\frac{\partial E}{\partial z} = \frac{1}{\varepsilon_0}(\rho_+ + \rho_-) \tag{B1}$$

First assume that the densities of the ions and electrons are low enough that recombination can be neglected. Then in quasi steady state the continuity equations for the ions and electrons are

$$\frac{\partial}{\partial z}\left(\rho_+ v_D^+\right) = \dot{q}$$

$$\frac{\partial}{\partial z}\left(\rho_- v_D^-\right) = -\dot{q} \tag{B2}$$

where $v_D^{\pm}$ are the ion and electron drift velocities. The density of ion/electron pairs produced per second by the incident ionizing radiation is $\dot{q}$ and assumed to be independent of distance between the plates. At atmospheric pressure the collision frequencies of ions and electrons with the gas molecules are high enough that they rapidly reach equilibrium drift velocities

$$v_D^+ = k_+ E$$

$$v_D^- = -k_- E \tag{B3}$$

where $k_{\pm}$ are the ion and electron mobilities. Multiplying Eqn. B1 by E and combining with Eqns. B2 and B3 gives

$$E\frac{\partial E}{\partial x} = \frac{1}{\varepsilon_0}\left(E\rho_+ + E\rho_-\right)$$

$$= \frac{1}{\varepsilon_0}\left(\frac{1}{k_+}v_D^+\rho_+ - \frac{1}{k_-}v_D^-\rho_-\right) \tag{B4}$$

$$\frac{1}{2}\frac{\partial}{\partial z}E^2 = \frac{1}{\varepsilon_0}\left(\frac{1}{k_+}v_D^+\rho_+ - \frac{1}{k_-}v_D^-\rho_-\right) \tag{B5}$$

33

$$\frac{\partial^2}{\partial z^2}E^2 = \frac{2}{\varepsilon_0}\left[\frac{1}{k_+}\frac{\partial}{\partial z}\left(v_D^+ \rho_+\right) - \frac{1}{k_-}\frac{\partial}{\partial z}\left(v_D^- \rho_-\right)\right]$$

$$= \frac{2}{\varepsilon_0}\left[\frac{\dot{q}}{k_+} + \frac{\dot{q}}{k_-}\right] \tag{B6}$$

$$= \frac{2\dot{q}}{\varepsilon_0 k_r}$$

where $k_r = \dfrac{k_+ k_-}{k_+ + k_-}$. Eqn. B6 is readily integrated to give

$$E^2 = \frac{\dot{q}}{\varepsilon_0 k_r}z^2 + Az + B \tag{B7}$$

where A and B are to be determined from the boundary conditions. If we let z = 0 be the anode and z = a the cathode then the charge densities obey the boundary conditions $\rho_+(0) = 0$, $\rho_-(a) = 0$. For Argon at 760 Torr the Ar^+ mobility is $k_+ = 1.7$ cm^2/V-sec. The electron mobility depends on field strength. For a typical value E = 1 kV/cm, $k_- = 500$ cm^2/V-sec. Since $k_- \gg k_+$ we will have $\rho_- \ll \rho_+$ throughout most of the ionization chamber. If we neglect ρ_- at z = 0 then from Poisson's Eqn. B1 we have $dE/dz(z=0) = 0$ and therefore A = 0. Then the field strength between plates is

$$E^2 = \frac{\dot{q}}{\varepsilon_0 k_r}z^2 + E_0^2. \tag{B8}$$

Looking at Eqn. B8 for a moment we see that in the low ionization density limit when the first term in Eqn. B8 is negligible the electric field between the plates is uniform and $E \approx E_0 = \dfrac{V}{a}$. In the opposite extreme, when the first term in Eqn. B8 is dominate, the electric field strength is linear in z. Within a factor of two the saturation condition Eqn. 15 is simply that the second term in Eqn. B8 be larger than the first with E_0 set to V_0/a.

From Eqn. B8 and E = - dV/dz we can write for the derivative of the voltage

$$\frac{\partial V}{\partial u} = -E_0 a\sqrt{1 + \zeta^2 u^2} \tag{B9}$$

34

where the u is the normalized distance between plates and a dimensionless space charge parameter ζ has been introduced

$$u = \frac{z}{a}$$

$$\zeta^2 = \frac{\dot{q}a^2}{\varepsilon_0 k_r E_0^2}$$

(B10)

Eqn. B9 may be integrated to give

$$V(u) = -\frac{E_0 a}{2\zeta}\left[\zeta u\sqrt{1+\zeta^2 u^2} + \log\left(\zeta u + \sqrt{1+\zeta^2 u^2}\right)\right]$$

(B11)

The boundary condition E_0 depends on the space charge density between the plates and therefore on $\dot{q}$ so it is convenient to introduce another dimensionless parameter ξ with V_0/a, which is independent of $\dot{q}$, taking the place of E_0.

$$\xi^2 = \frac{a^2}{V_0^2}E_0^2\zeta^2$$

$$= \frac{\dot{q}a^4}{\varepsilon_0 k_r V_0^2}$$

(B12)

Evaluating Eqn. B11 at $V(u = 1) = V_0$ yields the following relation between ζ and ξ

$$\frac{1}{\xi} = \frac{1}{2\zeta}\left[\sqrt{1+\zeta^2} + \frac{1}{\zeta}\log\left(\zeta + \sqrt{1+\zeta^2}\right)\right].$$

(B13)

For given $\dot{q}$, V_0, k_r and a Eqn. B13 determines the field strength E_0 at the cathode. At low ionization density, $\zeta - > 0, \xi - > \zeta$ and therefore $E_0 - > V_0/a$. At high ionization density $\zeta - > \infty, \xi - > 2$ and $E_0 - > 0$. The relationship between ζ and ξ is plotted in Fig. B1.

The complete solution for the voltage, field strength, charge densities and current density between the plates assuming recombination is negligible is

$$\frac{V(u)}{V_0} = -\frac{\xi}{2\zeta}\left[u\sqrt{1+\zeta^2 u^2} + \frac{1}{\zeta}\log\left(\zeta u + \sqrt{1+\zeta^2 u^2}\right)\right]$$

(B14)

35

$$E(u) = \frac{V_0}{a} \xi \sqrt{u^2 + \frac{1}{\zeta^2}} \tag{B15}$$

$$\rho_+(u) = \frac{\dot{q}a}{k_+ E(u)} u \tag{B16}$$

$$\rho_-(u) = -\frac{\dot{q}a}{k_- E(u)}(1-u)$$

$$\begin{aligned} j &= \rho_+(u)v_D^+ + \rho_-(u)v_D^- \\ &= \dot{q}a \end{aligned} \tag{B17}$$

The collection efficiency f_c is defined to be the ratio of ions collected to ions produced and according to Eqn. B17 is unity as it must be since recombination has been neglected
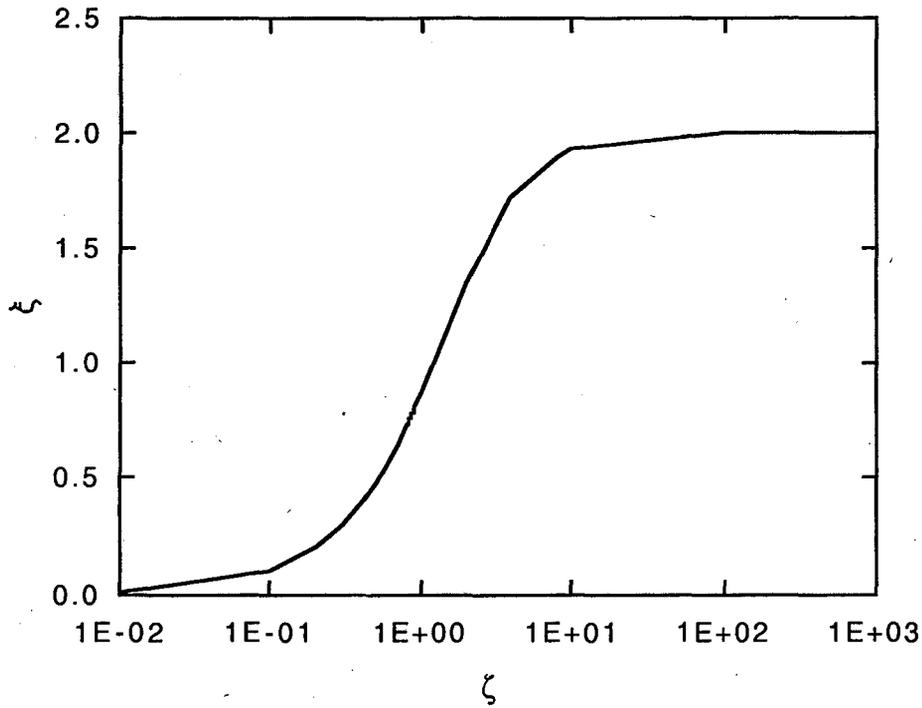
$$\begin{aligned} f_c &= \frac{j}{\dot{q}a} \\ &= 1 \end{aligned} \tag{B18}$$

We now examine the self consistency of Eqns. B14-17 and the assumption that recombination is negligible. In the presence of recombination the continuity Eqns. B2 are replaced by

$$\frac{\partial}{\partial z}\left(\rho_+ v_D^+\right) = \dot{q} - \dot{q}_r \tag{B19}$$

$$\frac{\partial}{\partial z}\left(\rho_- v_D^-\right) = -\dot{q} + \dot{q}_r$$

where the recombination current density is given by

$$\dot{q}_r = \frac{\alpha_r}{e} \rho_+ \rho_- \tag{B20}$$

36

Fig. B1: The relationship between the ionization density parameters ζ and ξ.

and α_r is the recombination coefficient. For Argon $\alpha_r = 3 \times 10^{-7}$ cm^3/sec.[8] In the presence of recombination the collection efficiency is

$$f_c = 1 - \frac{\int_0^a \dot{q}_r dz}{\dot{q}a}$$

$$= 1 - \frac{\alpha_r}{e} \frac{\dot{q}a^4}{k_+ k_-} \frac{1}{V_0^2} \frac{1}{\xi^2} \int_0^1 du \frac{u(1-u)}{u^2 + \frac{1}{\zeta^2}} .$$

$$= 1 - \frac{\alpha_r}{e} \frac{\dot{q}a^4}{k_+ k_-} \frac{1}{V_0^2} \frac{1}{\xi^2} I(\zeta)$$

(B21)

37

The charge densities given by Eqn. B16 have been substituted on the second line of Eqn. B21 and a dimensionless integral $I(\zeta)$ has been defined. According to Eqn. B13 the integral I can also be regarded as a function of ξ. For Eqns. B14-17 to be valid the recombination term in Eqn. B21 must be small compared to unity. The integral I is plotted versus ξ in Fig. B2 and we see that until ξ gets very close to 2, or equivalently E_0 gets very close to 0, $I \ll 1$. The combination of coefficients multiplying I in Eqn. B21 is also small compared to unity for typical parameter values. For example for $\alpha_r = 3\times10^{-7}$ cm^3/sec, $\dot{q} = 1\times10^{-6}$ A/cm^3, $k_+ = 1.7$ cm^2/V-sec, $k_- = 500$ cm^2/V-sec, a = 0.3 cm and $V_0 = 300$ V

$$\frac{\alpha_r}{e}\frac{\dot{q}a^4}{k_+k_-}\frac{1}{V_0^2} = 2.0\times10^{-4}.$$ (B22)

We therefore conclude that Eqns. B14-17 are valid for $\xi < 2.0$.
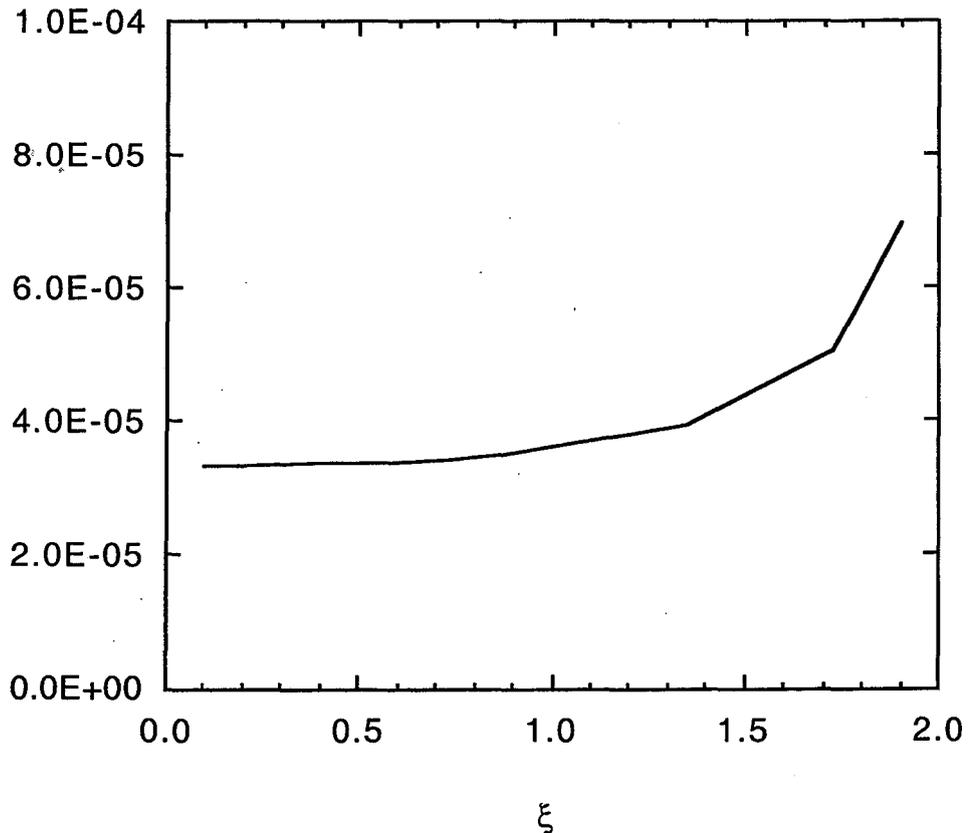
Fig. B2: The dimensionless recombination integral I versus ξ.

We now look at the solution for three regimes: (1) low space charge $\dot{q}->0, \zeta->0, \xi->0$, (2) intermediate space charge $\zeta->0, \xi->2, E(z=0)=0$ and (3) high space charge $\xi>2$. For $\dot{q}->0, \zeta->0, \xi->0$ we have from Eqns. B14-17

$$E = E_0 = \frac{V_0}{a}$$

$$V(u) = V_0 u$$

$$\rho_+(u) = \frac{\dot{q}a^2}{k_+V_0}u$$

$$\rho_-(u) = \frac{\dot{q}a^2}{k_-V_0}(1-u) \qquad\qquad \text{(B23)}$$

$$j = \rho_+(u)v_D^+ + \rho_-(u)v_D^-$$

$$= \dot{q}a$$

Eqns. B23 are very simple and what would be obtained by neglecting the ion and electron densities in Poisson's Eqn. B1. The ion (electron) density increases linearly with distance from the anode (cathode). Since $k_+ << k_-$ the space charge between the plates is dominated by the ions in the ratio $k_-/k_+ \sim 300$ for Argon and $E \sim 1$ kV/cm. If the ionization current density increases with the other parameters held fixed the ion space charge builds up to the point where it is no longer negligible and it starts to distort the electric field between the plates, suppressing the field at the anode and enhancing the field at the cathode. As $\xi->2$ the field at the cathode is suppressed to zero. For $\zeta->0, \xi->2, E(z=0)=0$ we obtain again from Eqns. B14-17

$$E(u) = 2\frac{V_0}{a}u$$

$$V(u) = -V_0 u^2$$

$$\rho_+ = \frac{1}{2}\frac{\dot{q}a^2}{k_+V_0} \qquad\qquad \text{(B24)}$$

$$\rho_- = -\frac{1}{2}\frac{\dot{q}a^2}{k_-V_0}\left(\frac{1}{u}-1\right)$$

$$j = \dot{q}a$$

where

$$\frac{\dot{q}a^4}{\varepsilon_0 k_r V_0^2} = 2^2 . \qquad\qquad \text{(B25)}$$

Comparing Eqns. B23 and B24 the potential V(u) between the plates changes from a linear to a parabolic function. The ion density in Eqn. B24 is constant between the plates and the electron density becomes divergent as the anode is approached. This divergence is artificial and due to the neglect of recombination and the strict requirement that E = 0 at z = 0. We will return to this below. For $\xi > 2$ the ionization current density $\dot{q}$ increases beyond that given by Eqn. B25 and the E $\approx$ 0 boundary moves off the anode and into the region between the plates. The width w of the E $\approx$ 0 layer is obtained by substitution of a - w for a in Eqn. B25.

$$\frac{\dot{q}(a-w)^4}{\varepsilon_0 k_r V_0^2} \equiv \xi^2 \left(1 - \frac{w}{a}\right)^2$$

$$= 2^2$$

(B26)

For 0 < z < w, we must have equality of the ion and electron charge densities $\rho_+ = \rho_-$ or otherwise the E $\approx$ 0 condition would be violated. Furthermore with vanishing electric field the ions and electrons created in this layer have negligible drift velocities and in steady state continuity requires that the ionization current density be balanced by recombination; $\dot{q} = \dot{q}_r$. We therefore obtain for $\xi > 2$ and 0 < z < w,

$$E(u) = 0$$

$$\rho_+(u) = -\rho_-(u)$$

$$= \sqrt{\frac{e\dot{q}}{\alpha}}$$

(B27)

For w < z < a the solution is the same as Eqn. B24 but with the anode to cathode gap reduced from a to a − w. The solution is obtained by substituting z − w for z and a − w for a in Eqn. B24.

$$E(u) = 2\frac{V_0}{a-w}\frac{u-\dfrac{w}{a}}{1-\dfrac{w}{a}}$$

$$V(u) = -V_0\left(\frac{u-\dfrac{w}{a}}{1-\dfrac{w}{a}}\right)^2$$

$$\rho_+ = \frac{1}{2}\frac{\dot{q}(a-w)^2}{k_+ V_0}$$

(B28)

$$\rho_- = -\frac{1}{2}\frac{\dot{q}(a-w)^2}{k_- V_0}\left(\frac{1-u}{u-\dfrac{w}{a}}\right)$$

The solutions for E and V are plotted versus u in Fig. B3 for ξ = 0.5, 2 and 8, characteristic of the three space charge regimes just discussed. Corresponding plots of ion and electron charge densities are given in Fig. B4.

For finite w, the current density falls below $\dot{q}a$ because of recombination in the E≈0 layer. From Eqn. B28 we calculate

$$j = \rho_+ v_D^+ + \rho_- v_D^-$$
$$= \dot{q}(a-w)$$

(B29)

and the collection efficiency is

$$f_c = \frac{j}{\dot{q}a}$$
$$= 1 \quad \xi \le 2.$$
$$= \sqrt{\frac{2}{\xi}} \quad \xi > 2$$

(B30)

The collection efficiency is plotted versus ξ is Fig. B5. The parametric dependence of the abscissa in Fig. B5 was deduced by Boag and Wilson[7] on the basis of dimensional analysis. The curve in Fig. B5 is in reasonable agreement with experimental data and applies to any gas ionization chamber for which negative ions are not formed by electron attachment. The condition for $f_c \approx 1$ is $\xi < 2$ or
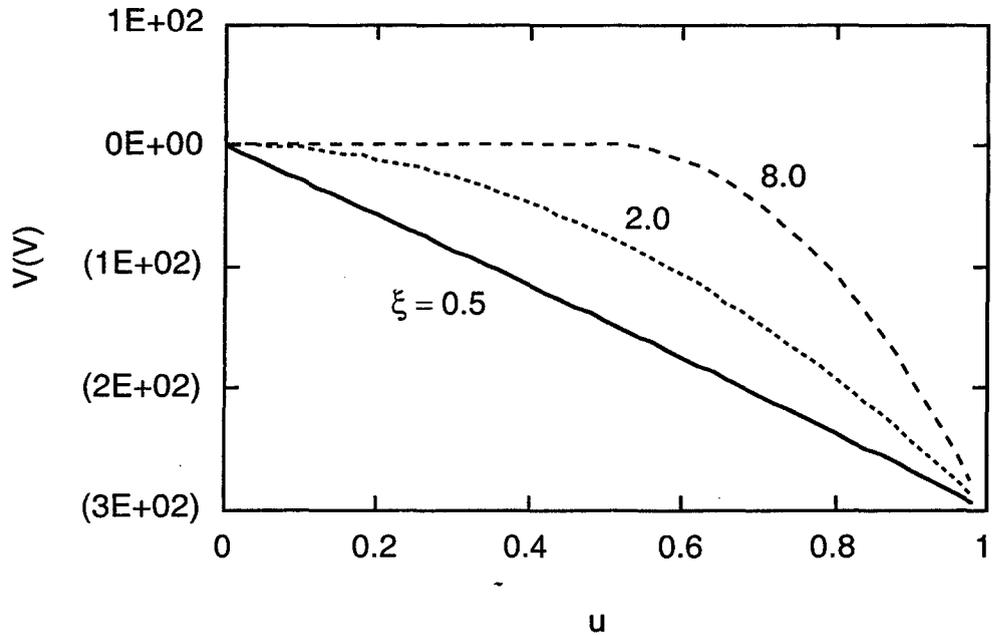
$$\frac{V_0}{a^2}\sqrt{\frac{\varepsilon_0 k_+}{\dot{q}}} \ge \frac{1}{2}$$

(B31)

which is the result given by Eqn. 15.

(a)

E(V/cm)

4E+03

3E+03

2E+03

1E+03

0E+00

ξ = 0.5

2.0   8.0

0.0   0.2   0.4   0.6   0.8   1.0

u

(b)

1E+02

0E+00

V(V)

(1E+02)

(2E+02)

(3E+02)

8.0

2.0

ξ = 0.5

0   0.2   0.4   0.6   0.8   1
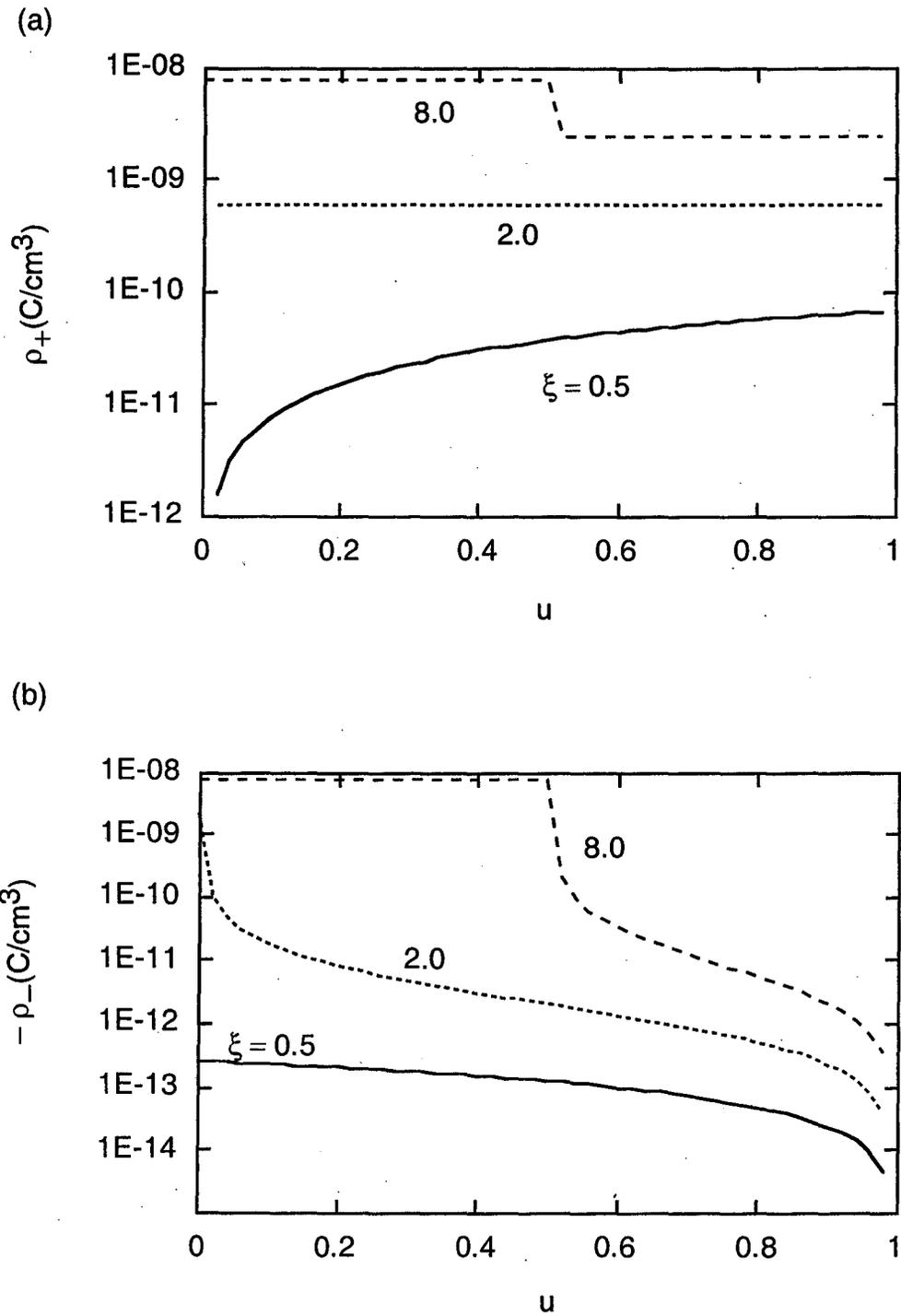
u
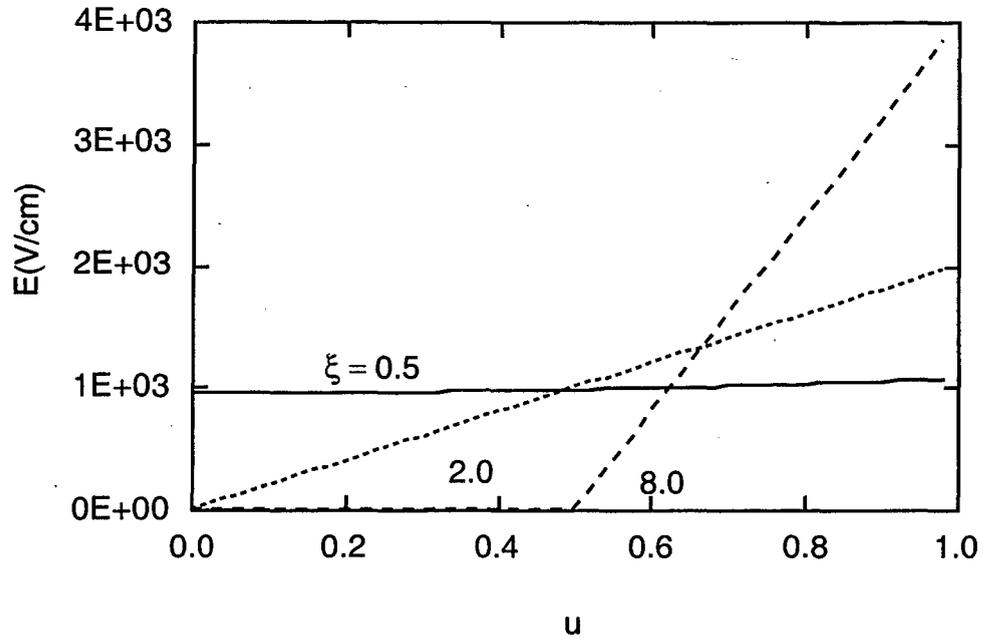
Fig. B3: (a) Electric field strength and (b) electric potential versus normalized distance u = z/a between the plates of an Argon ionization chamber for three values of the space charge parameter ξ = 0.5, 2 and 8.

(a)

(b)

Fig. B4: (a) Argon ion charge density and (b) electron charge density versus normalized distance $u = z/a$ between the plates of an Argon ionization chamber for three values of the space charge parameter ξ = 0.5, 2 and 8.

We note that the divergence of ρ_- to infinity as u $\rightarrow$ w/a in Eqns. B25 and B28 is artificial and is due to the neglect of recombination and the vanishing of the electric field at z = w. This is the same divergence that occurred in Eqn. B24 for ξ = 2, w = 0. The actual density is limited by the density given by Eqn. B27. The charge density given by Eqn. B27 is typically large compared to that in the un neutralized gap. Taking the ratio of electron density in Eqn. B27 to the ion density in Eqn. B28 in the limit w -> 0 for α = 3×10^{-7} cm^3/sec, $\dot{q} = 1 \times 10^{-6}$ A/cm^3, k_+ = 1.7 cm^2/V-sec, a = 0.3 cm and V_0 = 300 V we obtain

$$\lim_{w \to 0} \frac{\rho_\pm|_{0<z<w}}{\rho_+|_{w<z<a}} = \sqrt{\frac{e\dot{q}}{\alpha}} \frac{2k_+ V_0}{a^2} \, .$$

$$= 8.3$$

(B32)

If we set the magnitude of the divergent electron density equal to the ion density in Eqn. B28 we obtain an expression for the location where the electron density neutralizes the ion density

$$u = \frac{w}{a} + \frac{k_+}{k_-}\left(1 - \frac{w}{a}\right).$$

(B33)

Since $k_+/k_- \approx 1/300$ this neutralization occurs very close to the effective anode surface at u = w/a. The electric field strength where neutralization occurs can be obtained by substituting the expression for u in Eqn. B33 into Eqn. B28 and is small compared to the field strength in the un neutralized region, again because of the small value of k_+/k_-.

$$E(\rho_- = \rho_+) = \frac{k_+}{k_-} 2 \frac{V_0}{a - w}$$

$$\approx \frac{1}{300} 2 \frac{V_0}{a - w}$$

(B34)
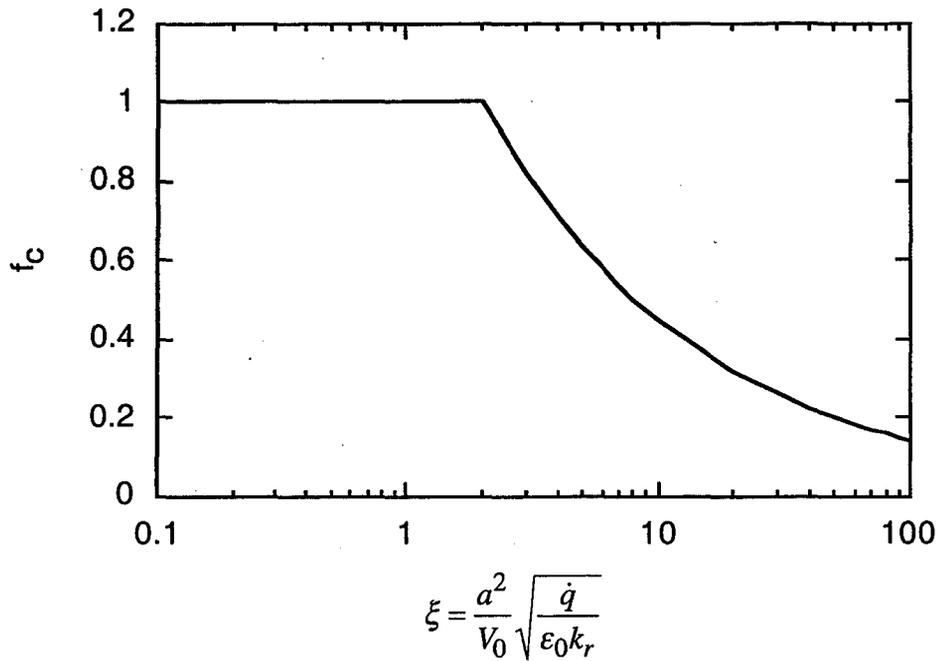
$$\xi = \frac{a^2}{V_0} \sqrt{\frac{\dot{q}}{\varepsilon_0 k_r}}$$

Fig. B5: The saturation curve for an Argon ionization chamber. Collection efficiency is plotted versus the space charge parameter

$$\xi = \frac{a^2}{V_0} \sqrt{\frac{\dot{q}}{\varepsilon_0 k_r}}.$$